

Performance Analysis and Resource Allocation of STAR-RIS Aided Wireless-Powered NOMA System

Kengyuan Xie, Guofa Cai, Georges Kaddoum, *Senior Member, IEEE*, Jiguang He,
Senior Member, IEEE

Abstract

This paper proposes a simultaneous transmitting and reflecting reconfigurable intelligent surface (STAR-RIS) aided wireless-powered non-orthogonal multiple access (NOMA) system, which includes an access point (AP), a STAR-RIS, and two non-orthogonal users located at both sides of the STAR-RIS. In this system, the users first harvest the radio-frequency energy from the AP in the downlink, then adopt the harvested energy to transmit information to the AP in the uplink concurrently. Two policies are considered for the proposed system. The first one assumes that the time-switching protocol is used in the downlink while the energy-splitting protocol is adopted in the uplink, named TEP. The second one assumes that the energy-splitting protocol is utilized in both the downlink and uplink, named EEP. The outage probability, sum throughput, and average age of information (AoI) of the proposed system with TEP and EEP are investigated over Nakagami- m fading channels. In addition, we also analyze the outage probability, sum throughput, and average AoI of the STAR-RIS aided wireless-powered time-division-multiple-access (TDMA) system. Simulation and numerical results show that the proposed system with TEP and EEP outperforms baseline schemes, and significantly improves sum throughput performance

K. Xie and G. Cai are with the School of Information Engineering, Guangdong University of Technology, China (e-mail: xiekengyuan@126.com, caiguofa2006@gdut.edu.cn).

G. Kaddoum is with the University of Québec, Québec, QCG1K 9H7, Canada, and also with École de Technologie Supérieure (ÉTS), LaCIME Laboratory, Montreal, QC H3C 1K3, Canada (e-mail: georges.kaddoum@etsmtl.ca).

J. He is with the Technology Innovation Institute, 9639 Masdar City, Abu Dhabi, United Arab Emirates (E-mail: jiguang.he@tii.ae).

but reduces outage probability and average AoI performance compared to the STAR-RIS aided wireless-powered TDMA system. Furthermore, to maximize the sum throughput and ensure a certain average AoI, we design a genetic-algorithm based time allocation and power allocation (GA-TAPA) algorithm. Simulation results demonstrate that the proposed GA-TAPA method can significantly improve the sum throughput by adaptively adjusting system parameters.

Index Terms

Wireless-powered communication (WPC), non-orthogonal multiple access (NOMA), simultaneous transmitting and reflecting reconfigurable intelligent surface (STAR-RIS), outage probability, sum throughput, age of information (AoI).

I. INTRODUCTION

Trillions of Internet-of-Things (IoT) devices will emerge, especially with the explosive growth of low-power devices, which will require a rethinking of future network design [1]. For the design of reliable and robust networks, the challenge of energy-constrained IoT devices is energy supply [2]. Recently, energy harvesting (EH) has been proposed as one of the most promising candidates to solve the energy-supply problem [3]. For example, harvesting energy from solar, piezoelectric, electromagnetic and other sources was proven to be effective for powering IoT devices [4]. In particular, radio frequency (RF) based EH provides an attractive solution to power low-power IoT devices over the air due to its flexible and reliable characteristics [5]. As a result, it enables wireless-powered communication (WPC) [6], which combines both wireless information transfer (WIT) and wireless power transfer (WPT) [7]. WPC has advantages in reducing the operational cost compared to conventional battery-powered counterparts and in improving the robustness of wireless communication networks especially low-power sensor networks. The major challenge of the WPC is the low transfer efficiency over a long distance [8]. Although the performance of WPC systems can be improved by adopting various existing techniques, e.g., relaying [9] and multiple-input multiple-output (MIMO) [10]. However, high energy consumption and hardware cost are introduced by these techniques due to signal amplification or regeneration and a large number of

RF chains.

Recently, reconfigurable intelligent surfaces (RISs), which can enhance spectrum efficiency, energy efficiency, and physical-layer security [11], have been proposed as one of the key technologies for the sixth-generation (6G) wireless networks [12], [13]. RIS, which consists of a large number of low-cost reflective elements, is an economical and energy-efficient technology compared to MIMO and relaying systems [13]. To improve the WPT efficiency and data rates of the WPC system, there has been a great interest in RIS aided WPC [14]–[17]. In [14], a RIS-assisted cooperative WPC network (WPCN) was proposed, where the RIS is utilized to improve the energy efficiency of the WPT phase and the spectrum efficiency of the WIT phase. In [15], a RIS aided wireless-powered sensor network was studied, where the RIS is deployed to enhance the sum throughput by intelligently adjusting the phase shift of each reflecting element. In [16], an energy buffer and RIS aided WPC system was proposed to improve the error performance. In [17], it was revealed that the doubly near-far issue in MIMO WPCN can be solved effectively with a rigorous deployment of the RIS.

However, the conventional RIS requires both the access point (AP) and user to be on the same side of the RIS [18]. To overcome this drawback, the concept of simultaneous transmitting and reflecting RIS (STAR-RIS) was proposed in [19], [20]. Different from conventional RIS, each element of STAR-RIS can transmit and reflect the incident signal simultaneously, thus breaking the location limitation of RIS deployment and achieving *full-space coverage* [21]. In STAR-RIS, one part of the incident signal is reflected to the same space as the incident signal, i.e., the reflection space, while the other part of the incident signal is transmitted to the opposite space, i.e., the transmission space [22]. Moreover, STAR-RIS provides a new degree-of-freedom for manipulating signal propagation, which increases the flexibility for network design [23]. To exploit the benefits of both WPC and STAR-RIS, a STAR-RIS-enhanced wireless-powered mobile edge computing system was proposed in [24], which was shown to improve the efficiency of energy transfer and task offloading by maximizing the total computation rate of all users. Furthermore, three practical protocols, including

energy-splitting, mode-switching, and time-switching, were presented in [22]. In the energy-splitting and mode-switching protocols, since the STAR-RIS splits the incident signal into two parts, a multiple access scheme need to be designed to distinguish these two parts for successful decoding [25]. Existing multiple access schemes feature two categories: orthogonal multiple access (OMA) and non-orthogonal multiple access (NOMA) [21]. Compared to OMA, NOMA can provide better spectrum efficiency and user fairness [26], [27]. Recently, several research efforts have focused on the performance analysis of STAR-RIS aided NOMA networks [23], [28]–[30]. In [23], the basic coverage of the STAR-RIS aided NOMA network was studied. In [28], the outage probability and diversity gains of a STAR-RIS aided downlink NOMA network with randomly deployed users were derived. In [29], the outage probability analysis of the STAR-RIS aided NOMA network over correlated channels was considered. In [30], the error performance of the STAR-RIS aided NOMA network was analyzed. In these existing STAR-RIS aided NOMA works [23], [28]–[30], the STAR-RIS is only deployed in the downlink transmissions. Actually, the STAR-RIS can be adopted in the uplink transmissions to improve the performance. However, the analytical methods of downlink transmissions for the STAR-RIS aided NOMA system can not be directly applicable for the uplink transmission.

With the aforementioned motivations, in this paper, we propose a STAR-RIS aided wireless-powered NOMA system, where the STAR-RIS is utilized to improve the efficiency of the WPT in the downlink and the performance of the WIT in the uplink. Moreover, we investigate the outage probability and sum throughput performance of the proposed system over Nakagami- m fading channels. Furthermore, the information freshness is essential for the IoT networks [31]. The age of information (AoI) is a metric for information freshness and plays a key role in real-time operations [32]. For this reason, we further analyze the average AoI of the proposed system. The contributions of this paper are summarized as follows:

- A STAR-RIS aided wireless-powered NOMA system is put forward, where the optimal decoding order policy for the successive interference cancellation (SIC) is considered instead of

following a specific decoding order. Moreover, two policies, i.e., TEP and EEP, are designed for the proposed system. Specifically, for the TEP, the time-switching and energy-splitting protocols are adopted in the downlink and uplink, respectively. For the EEP, the energy-splitting protocol is used in both the downlink and uplink.

- Based on the moment-matching approach, the outage probability and sum throughput expressions for the proposed system with TEP and EEP are derived over Nakagami- m fading channels. Moreover, to meet the timeliness requirements, the closed-form average AoI expressions of the proposed system with TEP and EEP is further investigated. In addition, the outage probability, sum throughput, and average AoI of the STAR-RIS aided wireless-powered time-division-multiple-access (TDMA) system are also analyzed. Simulation and numerical results show that the proposed system with TEP and EEP offers improved performance compared to baseline schemes, and significantly improves sum throughput performance but reduces outage probability and average AoI performance compared to the STAR-RIS aided wireless-powered TDMA system.
- To maximize the sum throughput and ensure a certain average AoI, a genetic-algorithm based time allocation and power allocation (GA-TAPA) algorithm, which jointly optimizes the time allocation and the power allocation, is proposed. Simulation results show that the proposed GA-TAPA method can provide a higher sum throughput performance by adaptively adjusting the system parameters.

The remainder of this paper is organized as follows. Section II introduces the system model. Section III analyzes the outage probability and sum throughput performance of the proposed system. Section IV carries out the average AoI analysis. Section V presents the proposed resource allocation scheme. Section VI presents the numerical results and discussions while Section VII concludes the paper.

II. SYSTEM MODEL

In this section, we describe the proposed STAR-RIS aided wireless-powered NOMA system. Two policies are considered for the proposed system, and their signal models are presented. Finally, we also introduce the STAR-RIS aided wireless-powered TDMA system.

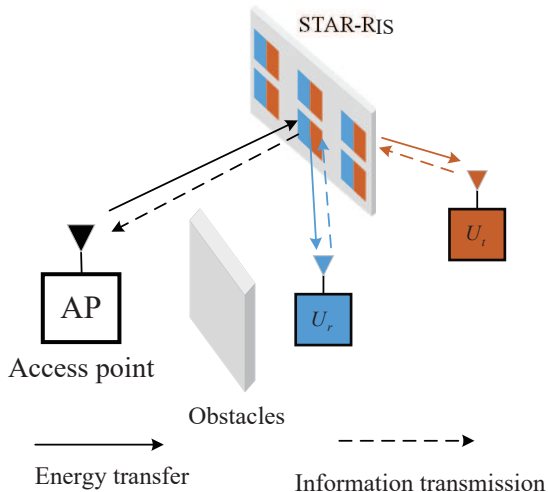


Fig. 1: STAR-RIS aided wireless-powered NOMA system model.

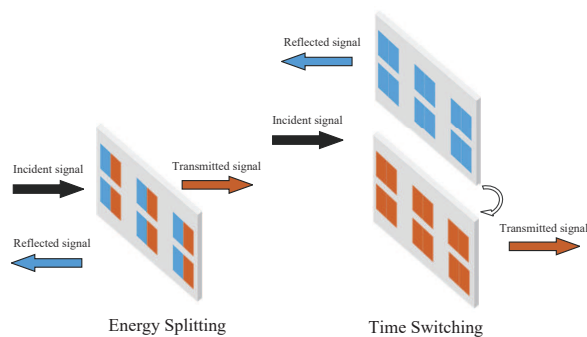


Fig. 2: Energy-splitting and time-switching protocols.

A. STAR-RIS Aided Wireless-Powered NOMA System

A STAR-RIS aided wireless-powered NOMA system is shown in Fig. 1, which consists of an AP, a STAR-RIS, and two users U_r and U_t . Here, AP, U_r , and U_t are equipped with a single antenna. In this system, it is assumed that there is a fixed energy supply for the AP. U_r and U_t are energy-constrained nodes and have to harvest the energy from the RF signal of the AP in the downlink. Then, in the uplink, U_r and U_t simultaneously transmit the backlogged data to the AP using the harvested energy in a NOMA fashion. The STAR-RIS, composed of N low-cost reflective elements, assists energy transfer (ET) from the AP to U_χ in the downlink and information transmission (IT) from the U_χ to AP in the uplink, where $\chi \in \{t, r\}$.

The energy-splitting and time-switching protocols are considered, as shown in Fig. 2. In TEP, the time-switching protocol is used in the uplink while the energy-splitting protocol is adopted in

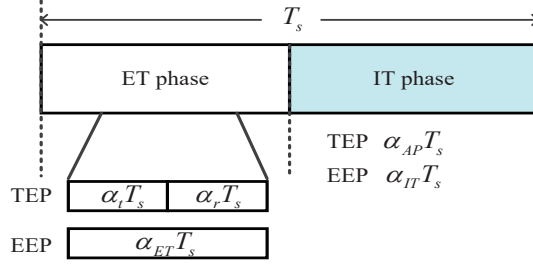


Fig. 3: ET and IT phases for the proposed system.

the downlink. Meanwhile, in EEP, the energy-splitting protocol is utilized in both the uplink and downlink.

The ET and IT phases of the TEP and EEP schemes are shown Fig. 3. In the TEP scheme, the total communication duration T_s is divided into three phases, where the ET phase for U_t is $\alpha_t T_s$, the ET phase for U_r is $\alpha_r T_s$, and the IT phase is $\alpha_{AP} T_s$, where the coefficients α_t , α_r , and α_{AP} satisfy $0 < \alpha_t, \alpha_r, \alpha_{AP} < 1$ and $\alpha_t + \alpha_r + \alpha_{AP} = 1$. In the EEP scheme, the duration of the ET phase is $\alpha_{ET} T_s$ and the duration of the IT phase is $\alpha_{IT} T_s$, where the coefficients α_{ET} and α_{IT} satisfy $0 < \alpha_{ET}, \alpha_{IT} < 1$ and $\alpha_{ET} + \alpha_{IT} = 1$. Without loss of generality, in this paper, we consider a normalized unit communication block time in the sequel, i.e., $T_s = 1$. The signal models of the TEP and EEP schemes are presented in the following.

B. TEP

1) *ET phase:* For the time-switching protocol, the STAR-RIS switches all elements between the transmission and reflection modes in different time periods. The ET phase is divided into two periods, i.e., the transmission period of duration $\alpha_t T_s$ for U_t and the reflection period of duration $\alpha_r T_s$ for U_r . Let $\varphi_{ET}^{TEP} \triangleq [e^{j\varphi_1^{TEP}}, \dots, e^{j\varphi_N^{TEP}}]$ and $\zeta_{ET}^{TEP} \triangleq [e^{j\zeta_1^{TEP}}, \dots, e^{j\zeta_N^{TEP}}]$ be the transmission and reflection coefficient vectors of the STAR-RIS, respectively, where φ_n^{TEP} and $\zeta_n^{TEP} \in [0, 2\pi)$ are the adjustable phase-shifts on the n -th element, $n \in \{1, 2, \dots, N\}$, j denotes the imaginary unit, i.e., $j^2 = -1$.

Let $\tilde{\mathbf{h}} \in \mathbb{C}^{1 \times N}$ denote the *complex channel coefficients* between the AP and STAR-RIS, $\tilde{\mathbf{g}}_r \in \mathbb{C}^{1 \times N}$ the *complex channel coefficients* between the STAR-RIS and U_r , and $\tilde{\mathbf{g}}_t \in \mathbb{C}^{1 \times N}$ the *complex*

channel coefficients between the STAR-RIS and U_t , where $\mathbb{C}^{1 \times N}$ is the space of $1 \times N$ complex-valued vectors. The path loss coefficient is $l_x = \frac{1}{d_0^{\vartheta_0} d_x^{\vartheta_x}}$, where d_0 and d_x are the distances from the AP to the STAR-RIS and from the STAR-RIS to U_x , respectively, and ϑ_0 and ϑ_x denote the corresponding path loss exponents.

In the transmission period, all the elements of the STAR-RIS are in transmission mode. The AP transmits the signals to U_t in the downlink. The received signal at U_t is given by

$$y_{t,TEP} = \sqrt{P_{AP} l_t} \tilde{\mathbf{h}} \text{diag}(\varphi_{ET}^{TEP}) \tilde{\mathbf{g}}_t^T s_{AP} + n_{t,TEP} = \sqrt{P_{AP} l_t} \left(\sum_{i=1}^N \tilde{h}_i e^{j\varphi_i^{TEP}} \tilde{g}_{t,i} \right) s_{AP} + n_{t,TEP}, \quad (1)$$

where P_{AP} denotes the transmitted power at the AP, $\text{diag}(\mathbf{X})$ is a diagonal matrix whose diagonals are the elements of \mathbf{X} , \mathbf{x}^T denotes the transpose of vector \mathbf{x} , s_{AP} is the signal that the AP transmits to U_t with $\text{E}\{|s_{AP}|^2\} = 1$, where $\text{E}(\cdot)$ represents the expectation operation, $n_{t,TEP} \sim \mathcal{CN}(0, N_0)$ is the additive white Gaussian noise (AWGN), where $\mathcal{CN}(\mu, \sigma^2)$ denotes the complex Gaussian distribution with mean μ and variance σ^2 .

The available energy at U_t can be calculated as

$$X_{t,TEP} = P_{AP} l_t \left| \sum_{i=1}^N \tilde{h}_i e^{j\varphi_i^{TEP}} \tilde{g}_{t,i} \right|^2 \alpha_t. \quad (2)$$

Moreover, the *complex channel coefficients* can be expressed in polar coordinates as $\tilde{h}_i = h_i e^{-j\mu_i}$ and $\tilde{g}_{t,i} = g_{t,i} e^{-j\sigma_i}$, where h_i and $g_{t,i}$ are the *magnitudes of the channel coefficients*, i.e., $|\tilde{h}_i| = h_i$ and $|\tilde{g}_{t,i}| = g_{t,i}$, and μ_i and σ_i are the *phases* of \tilde{h}_i and $\tilde{g}_{t,i}$, with $\{\mu_i, \sigma_i\} \in [0, 2\pi]$. The magnitudes of the channel coefficients follow a Nakagami- m distribution, i.e., $h_i \sim \text{Nakagami}(m_i, \Omega_i)$ and $g_{t,i} \sim \text{Nakagami}(m_{t,i}, \Omega_{t,i})$, where $m_i, m_{t,i}$ are the shape parameters that are larger than 0 and Ω_i and $\Omega_{t,i}$ are the spread parameters of the distribution. Hence, (2) can be expressed as

$$X_{t,TEP} = P_{AP} l_t \left| \sum_{i=1}^N h_i e^{j(\varphi_i^{TEP} - \mu_i - \sigma_i)} g_{t,i} \right|^2 \alpha_t. \quad (3)$$

To overcome the destructive effect of multipath fading, the phase-shifts of the STAR-RIS are reconfigured to obtain the maximum available energy. Considering perfect channel state information (CSI) [21], [22], the phase-shift of the STAR-RIS is set as $\varphi_i^{TEP} = \mu_i + \sigma_i$. Thus, (3) can be re-

expressed as $X_{t,TEP} = P_{AP} l_t \left| \sum_{i=1}^N h_i g_{t,i} \right|^2 \alpha_t$.

In the reflection period, all the elements of the STAR-RIS are in reflection mode. Similarly, the received signal at U_r is given by

$$y_{r,TEP} = \sqrt{P_{AP} l_r} \tilde{\mathbf{h}} \text{diag}(\zeta_{ET}^{TEP}) \tilde{\mathbf{g}}_r^T s_{AP} + n_{r,TEP} = \sqrt{P_{AP} l_r} \left(\sum_{i=1}^N \tilde{h}_i e^{j\zeta_i^{TEP}} \tilde{g}_{r,i} \right) s_{AP} + n_{r,TEP}, \quad (4)$$

where $n_{r,TEP} \sim \mathcal{CN}(0, N_0)$. The available energy is $X_{r,TEP} = P_{AP} l_r \left| \sum_{i=1}^N h_i g_{r,i} \right|^2 \alpha_r$, where $g_{r,i}$ also follows Nakagami $(m_{r,i}, \Omega_{r,i})$ with $m_{r,i}$ and $\Omega_{r,i}$ being the corresponding shape parameter and spread parameter of the distribution, respectively.

2) *IT Phase*: For the energy-splitting protocol, all the elements of the STAR-RIS work simultaneously in transmission and reflection modes with the energy-splitting ratios, i.e., $\sqrt{\beta_{t,TEP}}$ and $\sqrt{\beta_{r,TEP}} \in [0, 1]$. Accordingly, $\boldsymbol{\varphi}_{IT}^{TEP} \triangleq \left[\sqrt{\beta_{t,TEP}} e^{j\varphi_1^{TEP}}, \dots, \sqrt{\beta_{t,TEP}} e^{j\varphi_N^{TEP}} \right]$ and $\boldsymbol{\zeta}_{IT}^{TEP} \triangleq \left[\sqrt{\beta_{r,TEP}} e^{j\zeta_1^{TEP}}, \dots, \sqrt{\beta_{r,TEP}} e^{j\zeta_N^{TEP}} \right]$ denote the transmission and reflection coefficient vectors of the STAR-RIS, respectively. According to the law of energy conservation, $\beta_{t,TEP} + \beta_{r,TEP} = 1$ holds [21], [33].

In the IT phase, for the uplink NOMA system considered, U_t and U_r transmit data to the AP using the harvested energy over the same time and frequency resource block. The received signal at the AP is given by

$$y_{AP,TEP} = \sqrt{\frac{X_{t,TEP}}{\alpha_{AP}}} l_t \beta_{t,TEP} \left(\sum_{i=1}^N \tilde{h}_i e^{j\varphi_i^{TEP}} \tilde{g}_{t,i} \right) s_t + \sqrt{\frac{X_{r,TEP}}{\alpha_{AP}}} l_r \beta_{r,TEP} \left(\sum_{i=1}^N \tilde{h}_i e^{j\zeta_i^{TEP}} \tilde{g}_{r,i} \right) s_r + n_{AP}, \quad (5)$$

where s_χ is the signal from U_χ with $E\{|s_\chi|^2\} = 1$ and $n_{AP} \sim \mathcal{CN}(0, N_0)$.

The received signal-to-noise ratios (SNRs) of s_t and s_r are expressed as

$$\gamma_{t,TEP} = \frac{P_{AP} l_t^2 \beta_{t,TEP} \left| \sum_{i=1}^N h_i g_{t,i} \right|^4 \alpha_t}{\alpha_{AP} N_0}, \quad \gamma_{r,TEP} = \frac{P_{AP} l_r^2 \beta_{r,TEP} \left| \sum_{i=1}^N h_i g_{r,i} \right|^4 \alpha_r}{\alpha_{AP} N_0}. \quad (6)$$

The optimal decoding order policy for SIC is used to decode the received signal at the AP, given by [34]

$$S = \begin{cases} (t, r), & \frac{\gamma_{t,TEP}}{\gamma_{r,TEP+1}} \geq \gamma_{th} \& \frac{\gamma_{r,TEP}}{\gamma_{t,TEP+1}} < \gamma_{th} \\ (r, t), & \frac{\gamma_{t,TEP}}{\gamma_{r,TEP+1}} < \gamma_{th} \& \frac{\gamma_{r,TEP}}{\gamma_{t,TEP+1}} \geq \gamma_{th} \\ (t, r) \text{ or } (r, t), & \text{otherwise,} \end{cases} \quad (7)$$

where $\gamma_{th} = 2^R - 1$ with R being the target rate, $S = (x, y)$ denotes the decoding order that U_x is decoded before U_y .

C. EEP

For the EEP scheme, $\varphi^{EEP} \triangleq \left[\sqrt{\beta_{t,EEP}} e^{j\varphi_1^{EEP}}, \dots, \sqrt{\beta_{t,EEP}} e^{j\varphi_N^{EEP}} \right]$ and $\zeta^{EEP} \triangleq \left[\sqrt{\beta_{r,EEP}} e^{j\zeta_1^{EEP}}, \dots, \sqrt{\beta_{r,EEP}} e^{j\zeta_N^{EEP}} \right]$ are defined as the transmission and reflection coefficient vectors of the STAR-RIS, respectively.

1) *ET phase*: The received signal at U_t is given by

$$y_{t,EEP} = \sqrt{P_{AP} l_t \beta_{t,EEP}} \left(\sum_{i=1}^N \tilde{h}_i e^{j\varphi_i^{EEP}} \tilde{g}_{t,i} \right) s_{AP} + n_{t,EEP}. \quad (8)$$

The available energy at U_t can be calculated as

$$X_{t,EEP} = P_{AP} l_t \beta_{t,EEP} \left| \sum_{i=1}^N h_i g_{t,i} \right|^2 \alpha_{ET}. \quad (9)$$

Similarly, at U_r , one has

$$y_{r,EEP} = \sqrt{P_{AP} l_r \beta_{r,EEP}} \left(\sum_{i=1}^N \tilde{h}_i e^{j\zeta_i^{EEP}} \tilde{g}_{r,i} \right) s_{AP} + n_{r,EEP}, \quad (10)$$

and

$$X_{r,EEP} = P_{AP} l_r \beta_{r,EEP} \left| \sum_{i=1}^N h_i g_{r,i} \right|^2 \alpha_{ET}. \quad (11)$$

2) *IT Phase*: Similar to (5), the received signal at the AP can be expressed as

$$y_{AP,EEP} = \sqrt{\frac{X_{t,EEP}}{\alpha_{IT}} l_t \beta_{t,EEP}} \left(\sum_{i=1}^N \tilde{h}_i e^{j\varphi_i^{EEP}} \tilde{g}_{t,i} \right) s_t + \sqrt{\frac{X_{r,EEP}}{\alpha_{IT}} l_r \beta_{r,EEP}} \left(\sum_{i=1}^N \tilde{h}_i e^{j\zeta_i^{EEP}} \tilde{g}_{r,i} \right) s_r + n_{AP}. \quad (12)$$

The received SNRs of s_t and s_r are written as

$$\gamma_{t,EEP} = \frac{P_{AP} l_t^2 \beta_{t,EEP}^2 \left| \sum_{i=1}^N h_i g_{t,i} \right|^4 \alpha_{ET}}{\alpha_{IT} N_0}, \quad \gamma_{r,EEP} = \frac{P_{AP} l_r^2 \beta_{r,EEP}^2 \left| \sum_{i=1}^N h_i g_{r,i} \right|^4 \alpha_{ET}}{\alpha_{IT} N_0}. \quad (13)$$

Similar to the TEP scheme, for the uplink NOMA system considered, the EEP also uses the

optimal decoding order policy for SIC. One has

$$S = \begin{cases} (t, r), & \frac{\gamma_{t,EEP}}{\gamma_{r,EEP+1}} \geq \gamma_{th} \& \frac{\gamma_{r,EEP}}{\gamma_{t,EEP+1}} < \gamma_{th} \\ (r, t), & \frac{\gamma_{t,EEP}}{\gamma_{r,EEP+1}} < \gamma_{th} \& \frac{\gamma_{r,EEP}}{\gamma_{t,EEP+1}} \geq \gamma_{th} \\ (t, r) \text{ or } (r, t), & \text{otherwise.} \end{cases} \quad (14)$$

D. STAR-RIS Aided Wireless-Powered TDMA System

For OMA schemes, users are served by TDMA to avoid inter-user interference. The STAR-RIS operates in the time-switching protocol to support the downlink and uplink transmissions in a TDMA way. The ET phase is divided into $\alpha_t T_s$ for U_t and $\alpha_r T_s$ for U_r in the downlink, while the IT phase is divided into $\alpha_{AP}^t T_s$ for U_t and $\alpha_{AP}^r T_s$ for U_r in the uplink, where $\alpha_{AP}^t + \alpha_{AP}^r = 1 - \alpha_t - \alpha_r$. Hence, for the STAR-RIS aided wireless-powered TDMA system, the received SNR at U_χ is computed as

$$\gamma_\chi = \frac{P_{AP} l_\chi^2 \left| \sum_{i=1}^N h_i g_{\chi,i} \right|^4 \alpha_\chi}{\alpha_{AP}^\chi N_0}. \quad (15)$$

III. OUTAGE PROBABILITY AND SUM THROUGHPUT

In this section, the outage probability and sum throughput of the proposed system with the TEP and EEP, and the STAR-RIS aided wireless-powered TDMA system are derived over Nakagami- m fading channels.

Let $H_{h_i g_{t,i}} = h_i g_{t,i}$, the n -th moment of $H_{h_i g_{t,i}}$ is expressed as

$$\mu_{H_{h_i g_{t,i}}}(n) = \lambda_{h_i g_{t,i}}^{-n} \frac{\Gamma(m_i + n/2) \Gamma(m_{t,i} + n/2)}{\Gamma(m_i) \Gamma(m_{t,i})}, \quad (16)$$

where $\lambda_{h_i g_{t,i}} = \sqrt{\frac{m_i}{\Omega_i} \frac{m_{t,i}}{\Omega_{t,i}}}$, $\Gamma(\cdot)$ is the Gamma function. The detailed derivation of (16) is provided in Appendix A.

Here, the moment-matching approach is used to approximate the distribution of $H_{h_i g_{t,i}}$ with a Gamma distribution [29], [35], i.e., $H_{h_i g_{t,i}} \sim \text{Gamma}(k, \theta)$, where the k and θ is expressed as

$$k = \frac{\text{E}^2(H_{h_i g_{t,i}})}{\text{Var}(H_{h_i g_{t,i}})} = \frac{\mu_{H_{h_i g_{t,i}}}^2(1)}{\mu_{H_{h_i g_{t,i}}}(2) - \mu_{H_{h_i g_{t,i}}}^2(1)}, \theta = \frac{\text{E}(H_{h_i g_{t,i}})}{\text{Var}(H_{h_i g_{t,i}})} = \frac{\mu_{H_{h_i g_{t,i}}}(1)}{\mu_{H_{h_i g_{t,i}}}(2) - \mu_{H_{h_i g_{t,i}}}^2(1)}, \quad (17)$$

$\text{Var}(\cdot)$ represents the variance operation.

Let $G_{h_i g_{t,i}} = \sum_{i=1}^N h_i g_{t,i}$, one has $G_{h_i g_{t,i}} \sim \text{Gamma}(Nk, \theta)$. The cumulative distribution function (CDF) of $G_{h_i g_{t,i}}$ is expressed as

$$F_{G_{h_i g_{t,i}}}(x) = \frac{1}{\Gamma(Nk)} \gamma(Nk, \theta x), \quad (18)$$

where $\gamma(\cdot, \cdot)$ is the upper incomplete Gamma function.

For $Y = X^2$, the CDF of Y can be calculated as $F_Y(y) = F_X(\sqrt{y})$. The CDF of $|G_{h_i g_{t,i}}|^4$ is computed as

$$F_{|G_{h_i g_{t,i}}|^4}(x) = \frac{1}{\Gamma(Nk)} \gamma\left(Nk, \theta x^{\frac{1}{4}}\right) = 1 - \left(e^{-\theta x^{\frac{1}{4}}} + \sum_{m=1}^{Nk-1} e^{-\theta x^{\frac{1}{4}}} \frac{\theta^m x^{\frac{m}{4}}}{m!} \right). \quad (19)$$

The probability density function (PDF) of $|G_{h_i g_{t,i}}|^4$ is obtained as

$$f_{|G_{h_i g_{t,i}}|^4}(x) = \frac{\theta^{Nk} e^{-\theta x^{\frac{1}{4}}} x^{\frac{Nk-4}{4}}}{4(Nk-1)!}. \quad (20)$$

Let $G_{h_i g_{r,i}} = \sum_{i=1}^N h_i g_{r,i}$. The PDF and CDF of $G_{h_i g_{r,i}}$ are the same as those of $G_{h_i g_{t,i}}$. Hence, one has

$$F(x) = F_{|G_{h_i g_{r,i}}|^4}(x) = F_{|G_{h_i g_{t,i}}|^4}(x) = \frac{1}{\Gamma(Nk)} \gamma\left(Nk, \theta x^{\frac{1}{4}}\right), \quad (21)$$

$$f(x) = f_{|G_{h_i g_{r,i}}|^4}(x) = f_{|G_{h_i g_{t,i}}|^4}(x) = \frac{\theta^{Nk} e^{-\theta x^{\frac{1}{4}}} x^{\frac{Nk-4}{4}}}{4(Nk-1)!}. \quad (22)$$

A. TEP

According to the optimal decoding order policy in (7), the outage probability of U_t for the proposed system with the TEP scheme is given by

$$\begin{aligned} P_{out,t}^{\text{TEP}} &= \Pr\left(\frac{\gamma_{t,\text{TEP}}}{\gamma_{r,\text{TEP}} + 1} < \gamma_{th}, \frac{\gamma_{r,\text{TEP}}}{\gamma_{t,\text{TEP}} + 1} < \gamma_{th}\right) + \Pr\left(\gamma_{t,\text{TEP}} < \gamma_{th}, \frac{\gamma_{r,\text{TEP}}}{\gamma_{t,\text{TEP}} + 1} \geq \gamma_{th}\right) \\ &= F\left(\frac{\gamma_{th}}{B}\right) + \sum_{m=0}^{Nk-1} \frac{\theta^{Nk+m}}{4m!(Nk-1)!} \\ &\quad \times \left(\sum_{w=1}^W \psi_w e^{-\theta\left(\frac{B e^{u_w} + \gamma_{th}}{A \gamma_{th}} - \frac{1}{A}\right)^{\frac{1}{4}}} \left(\frac{B e^{u_w} + \gamma_{th}}{A \gamma_{th}} - \frac{1}{A}\right)^{\frac{m}{4}} e^{-\theta\left(e^{u_w} + \frac{\gamma_{th}}{B}\right)^{\frac{1}{4}}} \left(e^{u_w} + \frac{\gamma_{th}}{B}\right)^{\frac{Nk-4}{4}} e^{u_w + u_w^2} \right. \\ &\quad \left. - \sum_{w=1}^W \psi_w e^{-\theta\left(\frac{\gamma_{th}}{A}(B e^{u_w} + 1)\right)^{\frac{1}{4}}} \left(\frac{\gamma_{th}}{A}(B e^{u_w} + 1)\right)^{\frac{m}{4}} e^{-\theta e^{\frac{u_w}{4}}} e^{\frac{u_w Nk}{4} + u_w^2} \right. \\ &\quad \left. + \int_0^{\frac{\gamma_{th}}{A}} e^{-\theta\left(\frac{\gamma_{th}}{B}(Ax+1)\right)^{\frac{1}{4}}} \left(\frac{\gamma_{th}}{B}(Ax+1)\right)^{\frac{m}{4}} e^{-\theta x^{\frac{1}{4}}} x^{\frac{Nk-4}{4}} dx \right), \quad (23) \end{aligned}$$

where $A = \frac{P_{AP} I_t^2 \beta_{t,TEP} \alpha_t}{\alpha_{AP} N_0}$, $B = \frac{P_{AP} I_r^2 \beta_{r,TEP} \alpha_r}{\alpha_{AP} N_0}$. The detailed derivation of (23) is provided in Appendix B.

Similarly, the outage probability of U_r for the proposed system with the TEP scheme can be written as

$$\begin{aligned}
P_{out,r}^{TEP} &= \Pr\left(\frac{\gamma_{r,TEP}}{\gamma_{t,TEP} + 1} < \gamma_{th}, \frac{\gamma_{t,TEP}}{\gamma_{r,TEP} + 1} < \gamma_{th}\right) + \Pr\left(\gamma_{r,TEP} < \gamma_{th}, \frac{\gamma_{t,TEP}}{\gamma_{r,TEP} + 1} \geq \gamma_{th}\right) \\
&= F\left(\frac{\gamma_{th}}{A}\right) + \sum_{m=0}^{Nk-1} \frac{\theta^{Nk+m}}{4m!(Nk-1)!} \\
&\quad \times \left(\sum_{w=1}^W \psi_w e^{-\theta\left(\frac{Ae^{u_w} + \gamma_{th}}{B\gamma_{th}} - \frac{1}{B}\right)^{\frac{1}{4}}} \left(\frac{Ae^{u_w} + \gamma_{th}}{B\gamma_{th}} - \frac{1}{B}\right)^{\frac{m}{4}} e^{-\theta\left(e^{u_w} + \frac{\gamma_{th}}{A}\right)^{\frac{1}{4}}} \left(e^{u_w} + \frac{\gamma_{th}}{A}\right)^{\frac{Nk-4}{4}} e^{u_w + u_w^2} \right. \\
&\quad \times \left. - \sum_{w=1}^W \psi_w e^{-\theta\left(\frac{\gamma_{th}}{B}(Ae^{u_w} + 1)\right)^{\frac{1}{4}}} \left(\frac{\gamma_{th}}{B}(Ae^{u_w} + 1)\right)^{\frac{m}{4}} e^{-\theta e^{\frac{u_w}{4}}} e^{\frac{u_w Nk}{4} + u_w^2} \right. \\
&\quad \left. + \int_0^{\frac{\gamma_{th}}{A}} e^{-\theta\left(\frac{\gamma_{th}}{A}(Bx+1)\right)^{\frac{1}{4}}} \left(\frac{\gamma_{th}}{A}(Bx+1)\right)^{\frac{m}{4}} e^{-\theta x^{\frac{1}{4}}} x^{\frac{Nk-4}{4}} dx \right). \quad (24)
\end{aligned}$$

Finally, the sum throughput of the proposed system with the TEP scheme can be expressed as

$$T^{TEP} = R\alpha_{AP} (1 - P_{out,t}^{TEP}) + R\alpha_{AP} (1 - P_{out,r}^{TEP}). \quad (25)$$

B. EEP

According to (14), the outage probability of the proposed system with the EEP scheme is calculated as

$$\begin{aligned}
P_{out,\chi}^{EEP} &= F\left(\frac{\gamma_{th}}{D_\chi}\right) + \sum_{m=0}^{Nk-1} \frac{\theta^{Nk+m}}{4m!(Nk-1)!} \\
&\quad \times \left(\sum_{w=1}^W \psi_w e^{-\theta\left(\frac{D_\chi e^{u_w} + \gamma_{th}}{C_\chi \gamma_{th}} - \frac{1}{C_\chi}\right)^{\frac{1}{4}}} \left(\frac{D_\chi e^{u_w} + \gamma_{th}}{C_\chi \gamma_{th}} - \frac{1}{C_\chi}\right)^{\frac{m}{4}} e^{-\theta\left(e^{u_w} + \frac{\gamma_{th}}{D_\chi}\right)^{\frac{1}{4}}} \left(e^{u_w} + \frac{\gamma_{th}}{D_\chi}\right)^{\frac{Nk-4}{4}} e^{u_w + u_w^2} \right. \\
&\quad \times \left. - \sum_{w=1}^W \psi_w e^{-\theta\left(\frac{\gamma_{th}}{C_\chi}(D_\chi e^{u_w} + 1)\right)^{\frac{1}{4}}} \left(\frac{\gamma_{th}}{C_\chi}(D_\chi e^{u_w} + 1)\right)^{\frac{m}{4}} e^{-\theta e^{\frac{u_w}{4}}} e^{\frac{u_w Nk}{4} + u_w^2} \right. \\
&\quad \left. + \int_0^{\frac{\gamma_{th}}{D_\chi}} e^{-\theta\left(\frac{\gamma_{th}}{D_\chi}(C_\chi x + 1)\right)^{\frac{1}{4}}} \left(\frac{\gamma_{th}}{D_\chi}(C_\chi x + 1)\right)^{\frac{m}{4}} e^{-\theta x^{\frac{1}{4}}} x^{\frac{Nk-4}{4}} dx \right), \quad (26)
\end{aligned}$$

where $C_t = \frac{P_{AP} I_t^2 \beta_{t,EEP}^2 \alpha_{t,EEP}}{\alpha_{IT} N_0}$ and $D_t = \frac{P_{AP} I_r^2 \beta_{r,EEP}^2 \alpha_{r,EEP}}{\alpha_{IT} N_0}$ for U_t , and $C_r = \frac{P_{AP} I_r^2 \beta_{r,EEP}^2 \alpha_{r,EEP}}{\alpha_{IT} N_0}$ and $D_r = \frac{P_{AP} I_t^2 \beta_{t,EEP}^2 \alpha_{t,EEP}}{\alpha_{IT} N_0}$ for U_r .

Finally, the sum throughput of the proposed system with the EEP scheme can be expressed as

$$T^{EEP} = R\alpha_{IT} (1 - P_{out,t}^{EEP}) + R\alpha_{IT} (1 - P_{out,r}^{EEP}). \quad (27)$$

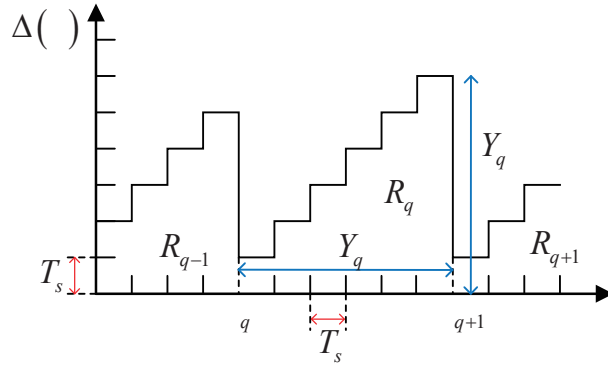


Fig. 4: Example of AoI.

C. STAR-RIS Aided Wireless-Powered TDMA System

For the STAR-RIS aided wireless-powered TDMA system, the outage probability of U_χ is given by

$$\begin{aligned}
 P_{out,\chi}^{TDMA} &= \Pr(\gamma_\chi < \gamma_{th}) = \Pr\left(\frac{P_{AP} l_\chi^2 \left|\sum_{i=1}^N h_i g_{\chi,i}\right|^4 \alpha_\chi}{\alpha_{AP}^\chi N_0} < \gamma_{th}\right) \\
 &= \Pr\left(\left|\sum_{i=1}^N h_i g_{\chi,i}\right|^4 < \frac{\gamma_{th} \alpha_{AP}^\chi N_0}{P_{AP} l_\chi^2 \alpha_\chi}\right) = F\left(\frac{\gamma_{th} \alpha_{AP}^\chi N_0}{P_{AP} l_\chi^2 \alpha_\chi}\right). \quad (28)
 \end{aligned}$$

The sum throughput of the STAR-RIS aided wireless-powered TDMA system can be expressed as

$$T^{TDMA} = R \alpha_{AP}^t (1 - P_{out,t}^{TDMA}) + R \alpha_{AP}^r (1 - P_{out,r}^{TDMA}). \quad (29)$$

IV. AGE OF INFORMATION

In this section, the average AoIs of the proposed system and the STAR-RIS aided wireless-powered TDMA system are analyzed. The duration of each communication process T_s , including the ET and IT phases, is employed to calculate the AoI. In time slot τ , the AoI of the system is defined as

$$\Delta(\tau) = \tau - U(\tau), \quad (30)$$

where $U(\tau)$ is the generation time of the most recently received packet at AP. Fig. 4 shows an example of the age evolution for the proposed system, where τ_q represents the time slot of the last time successful update at AP, τ_{q+1} represents the current time slot successfully updated at AP, and

$Y_q = \tau_{q+1} - \tau_q$ denotes the required time for the q -th successful update (time difference between τ_{q+1} and τ_q). If the decoding is successful, $\Delta(\tau)$ at AP is reset to one.

Firstly, we derive the first-order and second-order moments for the required time between two consecutive successful updates at AP, i.e., $Y_q \cdot Y_q = MT_s$, where M is a discrete random variable that denotes the number of consecutive communications until successful decoding. If M transmissions occur, this means that the previous $(M - 1)$ consecutive transmissions are unsuccessful, while the M -th transmission is successful [36]. According to ([37], eq. (1.113)), the expectation of Y_q can be calculated as

$$\mathbb{E}(Y_q) = \sum_{M=1}^{\infty} M \mathbb{E}(T_s) (1 - \Phi)^{M-1} \Phi = \frac{1}{\Phi}, \quad (31)$$

where $\mathbb{E}(T_s) = 1$ and Φ is the success probability.

For the second-order moment of Y_q , one has $Y_q^2 = M^2 T_s^2$. Since M is a discrete random variable, by taking the conditional expectation operator of Y_q^2 , one obtains $\mathbb{E}(Y_q^2 | M) = M^2 \mathbb{E}(T_s^2)$.

Similar to ([36], eq. (20)), the second-order moment of Y_q is calculated as

$$\mathbb{E}(Y_q^2) = \sum_{M=1}^{\infty} \mathbb{E}(Y_q^2 | M) (1 - \Phi)^{M-1} \Phi = \mathbb{E}(T_s^2) \left(\frac{2}{\Phi^2} - \frac{1}{\Phi} \right) = \frac{2}{\Phi^2} - \frac{1}{\Phi}, \quad (32)$$

where $\mathbb{E}(T_s^2) = 1$.

For a time period of η time slots in which κ status updates occur, the average time Δ_η of the proposed system is given by

$$\Delta_\eta = \frac{1}{\eta} \sum_{\tau=1}^{\eta} \Delta(\tau) = \frac{1}{\eta} \sum_{q=1}^{\kappa} R_q = \frac{\kappa}{\eta} \frac{1}{\kappa} \sum_{q=1}^{\kappa} R_q, \quad (33)$$

where R_q denotes the area under $\Delta(\tau)$ corresponding to the q -th status update. When η tends to infinity, the average time Δ_η tends to the average AoI [38], i.e.,

$$\Delta = \lim_{\eta \rightarrow \infty} \Delta_\eta = \lim_{\eta \rightarrow \infty} \frac{\kappa}{\eta} \frac{1}{\kappa} \sum_{q=1}^{\kappa} R_q = \lim_{\eta \rightarrow \infty} \frac{\kappa}{\eta} \frac{1}{\kappa} \mathbb{E}(R_q) = \frac{\mathbb{E}(R_q)}{\mathbb{E}(Y_q)}, \quad (34)$$

where $\lim_{\eta \rightarrow \infty} \frac{\kappa}{\eta} = \frac{1}{\mathbb{E}(Y_q)}$ [36].

The area R_q consists of Y_q rectangles. One side of the rectangle is one and another side is ℓ ,

where $1 \leq \ell \leq Y_q$. As shown in Fig. 4, one has $R_q = \sum_{\ell=1}^{Y_q} \ell = \frac{Y_q(Y_q+1)}{2}$. Taking the expectation of R_q , one has $E(R_q) = \frac{E(Y_q^2) + E(Y_q)}{2}$. Thus, the average AoI is calculated as

$$\Delta = \frac{1}{2} \left(\frac{E(Y_q^2)}{E(Y_q)} + 1 \right) = \frac{1}{2} \left(\frac{\frac{2}{\Phi^2} - \frac{1}{\Phi}}{\frac{1}{\Phi}} + 1 \right) = \frac{1}{\Phi}. \quad (35)$$

The success probability Φ_{TEP} for the TEP scheme is given by

$$\begin{aligned} \Phi_{TEP} &= \sum_{m=0}^{Nk-1} \frac{\theta^{Nk}}{4(Nk-1)!m!} \\ &\times \left(\sum_{w=1}^W \psi_w e^{-\left(\frac{\theta^4 \gamma_{th} U_3}{U_1}\right)^{\frac{1}{4}}} \left(\frac{\theta^4 \gamma_{th} U_3}{U_1}\right)^{\frac{m}{4}} e^{-\theta \left(e^{u_w} + \frac{\gamma_{th} \alpha_{AP} N_0}{U_2}\right)^{\frac{1}{4}}} \left(e^{u_w} + \frac{\gamma_{th} \alpha_{AP} N_0}{U_2}\right)^{\frac{Nk-4}{4}} e^{u_w + u_w^2} \right. \\ &\left. + \sum_{w=1}^W \psi_w e^{-\left(\frac{\theta^4 \gamma_{th} U_4}{U_2}\right)^{\frac{1}{4}}} \left(\frac{\theta^4 \gamma_{th} U_4}{U_2}\right)^{\frac{m}{4}} e^{-\theta \left(e^{u_w} + \frac{\gamma_{th} \alpha_{AP} N_0}{U_1}\right)^{\frac{1}{4}}} \left(e^{u_w} + \frac{\gamma_{th} \alpha_{AP} N_0}{U_1}\right)^{\frac{Nk-4}{4}} e^{u_w + u_w^2} \right) + 2O_W, \quad (36) \end{aligned}$$

where $U_1 = P_{AP} l_r^2 \beta_{r,TEP} \alpha_r$, $U_2 = P_{AP} l_t^2 \beta_{t,TEP} \alpha_t$, $U_3 = U_2 e^{u_w} + \gamma_{th} \alpha_{AP} N_0 + \alpha_{AP} N_0$, and $U_4 = U_1 e^{u_w} + \gamma_{th} \alpha_{AP} N_0 + \alpha_{AP} N_0$. The detailed derivation of (36) is provided in Appendix C.

Similarly, the success probability Φ_{EEP} for the EEP scheme can be calculated as

$$\begin{aligned} \Phi_{EEP} &= \sum_{m=0}^{Nk-1} \frac{\theta^{Nk}}{4(Nk-1)!m!} \\ &\times \left(\sum_{w=1}^W \psi_w e^{-\left(\frac{\theta^4 \gamma_{th} (V_3)}{V_1}\right)^{\frac{1}{4}}} \left(\frac{\theta^4 \gamma_{th} (V_3)}{V_1}\right)^{\frac{m}{4}} e^{-\theta \left(e^{u_w} + \frac{\gamma_{th} \alpha_{IT} N_0}{V_2}\right)^{\frac{1}{4}}} \left(e^{u_w} + \frac{\gamma_{th} \alpha_{IT} N_0}{V_2}\right)^{\frac{Nk-4}{4}} e^{u_w + u_w^2} \right. \\ &\left. + \sum_{w=1}^W \psi_w e^{-\left(\frac{\theta^4 \gamma_{th} (V_4)}{V_2}\right)^{\frac{1}{4}}} \left(\frac{\theta^4 \gamma_{th} (V_4)}{V_2}\right)^{\frac{m}{4}} e^{-\theta \left(e^{u_w} + \frac{\gamma_{th} \alpha_{IT} N_0}{V_1}\right)^{\frac{1}{4}}} \left(e^{u_w} + \frac{\gamma_{th} \alpha_{IT} N_0}{V_1}\right)^{\frac{Nk-4}{4}} e^{u_w + u_w^2} \right) + 2O_W, \quad (37) \end{aligned}$$

where $V_1 = P_{AP} l_r^2 \beta_{r,EEP}^2 \alpha_{ET}$, $V_2 = P_{AP} l_t^2 \beta_{t,EEP}^2 \alpha_{ET}$, $V_3 = V_2 e^{u_w} + \gamma_{th} \alpha_{IT} N_0 + \alpha_{IT} N_0$, and $V_4 = V_1 e^{u_w} + \gamma_{th} \alpha_{IT} N_0 + \alpha_{IT} N_0$.

The success probability Φ_T for the STAR-RIS aided wireless-powered TDMA system is given by

$$\begin{aligned} \Phi_T &= 2 - \sum_{m=0}^{Nk-1} \frac{\theta^{m+Nk} U_5^{\frac{m}{4}}}{m!(Nk-1)!} \left(\theta \left(U_5^{\frac{1}{4}} + 1 \right) \right)^{-(Nk+m)} \Gamma(Nk+m) - \sum_{m=0}^{Nk-1} \frac{\theta^{m+Nk} U_6^{\frac{m}{4}}}{m!(Nk-1)!} \\ &\times \left(\theta \left(U_6^{\frac{1}{4}} + 1 \right) \right)^{-(Nk+m)} \Gamma(Nk+m) - F \left(\frac{\gamma_{th} \alpha_{AP}^t N_0}{P_{AP} l_t^2 \alpha_t} \right) - F \left(\frac{\gamma_{th} \alpha_{AP}^r N_0}{P_{AP} l_r^2 \alpha_r} \right), \quad (38) \end{aligned}$$

where $U_5 = \frac{l_r^2 \alpha_r \alpha_{AP}^t}{\alpha_{AP}^r l_t^2 \alpha_t}$, $U_6 = \frac{l_t^2 \alpha_t \alpha_{AP}^r}{\alpha_{AP}^t l_r^2 \alpha_r}$. The detailed derivation of (38) is provided in Appendix C.

V. RESOURCE ALLOCATION

In this section, resource allocation is analyzed to maximize the sum throughput within an average AoI constraint.

A. Problem Formulation

1) *TEP*: We formulate the sum throughput problem as an optimization problem seeking to jointly optimize the time allocation and power allocation, subject to the average AoI requirement. From (23), (24), and (25), the time-allocation parameters are α_t , α_r , and α_{AP} , and the power-allocation parameters are $\beta_{t,TEP}$ for U_t and $\beta_{r,TEP}$ for U_r . From (35), the average AoI for the TEP scheme is $\Delta_{TEP} = \frac{1}{\Phi_{TEP}}$.

The optimization problem can be formulated as

$$\mathcal{P}_1 : \quad \max_{\substack{\alpha_t, \alpha_r, \alpha_{AP} \\ \beta_{t,TEP}, \beta_{r,TEP}}} T^{TEP}(\alpha_t, \alpha_r, \alpha_{AP}, \beta_{t,TEP}, \beta_{r,TEP}) \quad (39)$$

$$s.t. \quad C1 : 0 < \alpha_t, \alpha_r, \alpha_{AP} < 1, \quad (39a)$$

$$C2 : \alpha_t + \alpha_r + \alpha_{AP} = 1, \quad (39b)$$

$$C3 : 0 < \beta_{t,TEP}, \beta_{r,TEP} < 1, \quad (39c)$$

$$C4 : \beta_{t,TEP} + \beta_{r,TEP} = 1, \quad (39d)$$

$$C5 : \Delta_{TEP} = \frac{1}{\Phi_{TEP}} < \Delta_{th}. \quad (39e)$$

Constraint (39a) specifies the range of α_t , α_r , and α_{AP} . Constraint (39b) illustrates the relationship between α_t , α_r and α_{AP} . To simplify the analysis, let α_t and α_r be equal, i.e., $\alpha_t = \alpha_r = \frac{(1-\alpha_{AP})}{2}$. Constraint (39c) ensures the range of energy-splitting ratios of the STAR-RIS, i.e., the range of power-allocation ratios for each user. Constraint (39d) is set to satisfy the law of energy conservation. Constraint (39e) guarantees that the average AoI is less than the preset threshold Δ_{th} .

2) *EEP*: For the EEP scheme, the joint time allocation and power allocation optimization problem, subject to average AoI, can be formulated as

$$\mathcal{P}_2 : \quad \max_{\substack{\alpha_{ET}, \alpha_{IT} \\ \beta_{t,EEP}, \beta_{r,EEP}}} T^{EEP}(\alpha_{ET}, \alpha_{IT}, \beta_{t,EEP}, \beta_{r,EEP}) \quad (40)$$

$$s.t. \quad C1 : 0 < \alpha_{ET}, \alpha_{IT} < 1, \quad (40a)$$

$$C2 : \alpha_{ET} + \alpha_{IT} = 1, \quad (40b)$$

$$C3 : 0 < \beta_{t,EEP}, \beta_{r,EEP} < 1, \quad (40c)$$

$$C4 : \beta_{t,EEP} + \beta_{r,EEP} = 1, \quad (40d)$$

$$C5 : \Delta_{EEP} = \frac{1}{\Phi_{EEP}} < \Delta_{th}. \quad (40e)$$

Constraints (40a) and (40b) specify the range and relationship between α_{ET} and α_{IT} . Constraint (40c) ensures the range of energy-splitting ratios of the STAR-RIS, i.e., the range of power-allocation ratios for each user. Constraint (40d) is set to satisfy the law of energy conservation. Constraint (40e) guarantees that the average AoI is less than the preset threshold Δ_{th} .

B. Proposed Algorithm

\mathcal{P}_1 and \mathcal{P}_2 aim to maximize the sum throughput, which is related to the outage probability. Since the outage probability expression is intractable, the derivative-free optimization method is considered to obtain the optimal solution. Moreover, as the scale of the network grows, it is difficult for the optimization problem to be solved in an acceptable amount of time using an exhaustive search method. Therefore, the genetic-algorithm (GA) based time allocation and power allocation (GA-TAPA) method is proposed to solve \mathcal{P}_1 and \mathcal{P}_2 . The details of the proposed GA-TAPA method is summarized in Algorithm 1.

The GA is a meta-heuristic algorithm and an efficient global optimization method, which adopts the idea of survival of the fittest as its evolution principle to reach the optimal solution [39], [40]. With the proposed GA-TAPA algorithm, which keeps the feature of GA, the numerical optimized results can be obtained. This derivative-free optimization is practical because it does not require the computation of gradients [41].

The time complexity of the proposed algorithm is calculated. Here, binary coded GA is used. Ξ

is defined as the bit length of the binary code and chromosome length. We give the time complexity of each process and compute the overall complexity of the proposed algorithm. According to the population size ε and the chromosome length Ξ , the time complexity of initializing the population is given by $O(\varepsilon \times \Xi)$. The time complexity of fitness evaluation for the maximum generation G_{en} is $O(\varepsilon \times G_{en})$. The time complexity of the selection operation, crossover operation, and mutation operation is $O(\varepsilon^2 \times G_{en}) + O(\varepsilon \times G_{en}) + O(\varepsilon \times G_{en}) \approx O(\varepsilon^2 \times G_{en})$. Hence, the overall time complexity of the proposed GA-TAPA algorithm is approximated as $O(\varepsilon^2 \times G_{en})$.

Algorithm 1 Genetic-Algorithm Based Time Allocation and Power Allocation (GA-TAPA)

Input: The size of the population ε , the iteration of GA-TAPA G_{en} , the parameters of GA q_t, p_t, p_m .

Output: $\alpha_t, \alpha_r, \alpha_{AP}, \beta_{t,TEP}, \beta_{r,TEP}$ for the TEP scheme or $\alpha_{ET}, \alpha_{IT}, \beta_{t,EEP}, \beta_{r,EEP}$ for the EEP scheme.

- 1: Randomly initialize the population based on ε , (39a), (39b), (39c), (39d) for the TEP, or ε , (40a), (40b), (40c), (40d) for the EEP.
 - 2: **for** $i = 1 : G_{en}$ **do**
 - 3: Evaluate the population, i.e., calculate the penalty fitness value of the individuals according to (39) and (39e) for the TEP scheme or (40) and (40e) for the EEP scheme.
 - 4: Rank the individuals according to their penalty fitness values. Select the father generations with the selection probability q_t and randomly select mother generation.
 - 5: Crossover the father and mother generations with the crossover probability p_t to generate new population.
 - 6: For each individual, do the mutation operation with the mutation probability p_m .
 - 7: Update population.
 - 8: **end for**
 - 9: Calculate the fitness value of the population and find the best fitness individual.
-

VI. RESULTS AND DISCUSSION

In this section, the outage probability, sum throughput and average AoI of the proposed STAR-RIS aided wireless-powered NOMA system are evaluated, where the TEP and EEP are considered. In the simulations, $P_{AP} = 1$ Watt (W). The parameters of the path loss are set as follows: $d_0 = 30$ m, $d_r = 4$ m, $d_t = 2$ m, and $\vartheta_0 = \vartheta_\chi = 2$. Moreover, unless stated otherwise, it is assumed that $\beta_{r,TEP} = \beta_{r,EEP} = 0.4$, $\beta_{t,TEP} = \beta_{t,EEP} = 0.6$, $\alpha_t = \alpha_r = 0.25$, $\alpha_{AP} = 0.5$, $\alpha_{ET} = 0.5$, and $\alpha_{IT} = 0.5$. Regarding the Nakagami- m fading channel parameters, we assume $m_i = m_{t,i} = m_{r,i} = 2$ and $\Omega_i = \Omega_{t,i} = \Omega_{r,i} = 1$. To demonstrate the advantages of the proposed system, conventional RIS (C-RIS) schemes are considered as baseline schemes for comparison purposes. For one C-RIS scheme, a reflecting-only RIS and a transmitting-only RIS at the same location of the STAR-RIS are

deployed to achieve full-space coverage, where each reflecting/transmitting-only RIS is equipped with $\frac{N}{2}$ elements [42]. Furthermore, both C-RIS wireless-powered NOMA (C-RIS-NOMA) and C-RIS wireless-powered TDMA (C-RIS-TDMA) schemes are considered. In addition, the STAR-RIS aided wireless-powered TDMA system is referred to as STAR-RIS-TDMA.

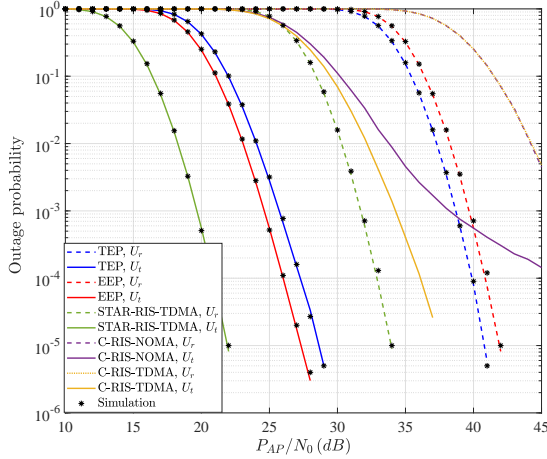


Fig. 5: Outage probability versus transmit SNR of various systems, where $N = 30$ and $R = 1$.

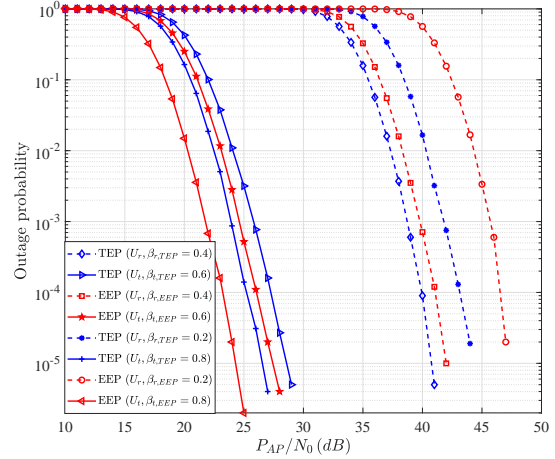


Fig. 6: Outage probability of the proposed system with the TEP and EEP schemes for different power allocation coefficients, where $N = 30$ and $R = 1$.

Fig. 5 shows the outage probability versus transmit SNR of various systems, where $N = 30$ and $R = 1$. In this figure, theoretical results are consistent with the simulation results, which validates the proposed analyses. It can be observed that the proposed system shows better outage probability performance than the C-RIS-NOMA and C-RIS-TDMA systems. The reason behind that is that STAR-RIS can configure full-space electromagnetic propagation environments while the conventional RIS needs a reflecting-only RIS and a transmitting-only RIS to achieve full-space coverage. Compared to the C-RIS, the STAR-RIS has more adjustable parameters to adjust the channel conditions of users. Moreover, it can be seen that the outage probability performance of the STAR-RIS-TDMA scheme is better than that of the proposed scheme, because inter-user interference occurs in the proposed scheme. Furthermore, it can be seen that for U_t , the EEP scheme shows better performance than the TEP scheme; while for U_r , the TEP scheme performs better compared to the EEP scheme. This is because the EEP scheme allocates more resources to U_t , while the TEP scheme balances the energy harvested by the two users in the downlink to

reduce the performance gap.

Fig. 6 depicts the outage probability of the proposed system with the TEP and EEP schemes for different power allocation coefficients. It is observed that U_r is more sensitive to changes in the power allocation compared to U_t . For example, for the EEP scheme, an increment of 0.2 in the power allocation results in a 6 dB gain for U_r while U_t can only achieve a 3 dB gain at an outage probability of 10^{-4} . This is because U_r is a far-side user, where more power allocation helps U_r significantly improve its performance and reduce the double near-far impact, which indicates that the far user harvests less energy, but needs more energy to transmit information during the uplink. Moreover, it can be seen that the EEP scheme is more sensitive to changes in the power allocation compared to the TEP scheme due to the energy-splitting protocol in both uplink and downlink.

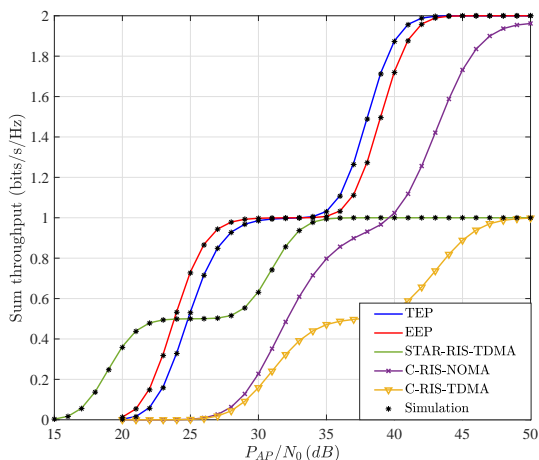


Fig. 7: Sum throughput versus transmit SNR for various systems, where $N = 30$ and $R = 2$.

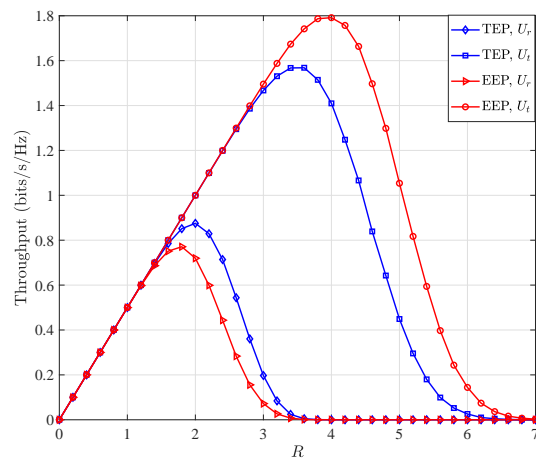


Fig. 8: Throughput versus R for the proposed system with the TEP and EEP schemes, where $N = 30$ and $\frac{P_{AP}}{N_0} = 40$ dB.

Fig. 7 illustrates the sum throughput versus transmit SNR of various systems, where $N = 30$ and $R = 2$. It can be observed that the proposed system shows better sum throughput performance than the baseline and STAR-RIS-TDMA schemes. The reason behind this is that NOMA allows U_t and U_r to use the same time-frequency resource block, thus achieving a multiplexing gain compared to TDMA, and NOMA allows the STAR-RIS to exploit the proper power allocation to achieve better performance. At low SNR, the performance of STAR-RIS-TDMA is a slightly better than that of the proposed system with the TEP and EEP schemes. This is because the TEP and EEP

schemes use the energy-splitting protocol in the uplink, thus causing opposite-side leakage, which indicates that some of the uplink signals of U_r are transmitted and some of the uplink signals of U_t are reflected. Moreover, it can be seen that there is an intersection point between the C-RIS-NOMA and STAR-RIS-TDMA curves. This is because at low SNR, the beamforming gain of the STAR-RIS is more prominent while at high SNR, the multiplexing gain increases and eventually exceeds the beamforming gain to become the dominant factor [42]. Furthermore, it can be seen that the sum throughput performance of the EEP scheme is better than that of the TEP scheme at low SNR while the TEP outperforms the EEP at high SNR. The reason behind this is that the outage probability of the EEP scheme is better at low SNR while the outage probability of the TEP scheme is better at high SNR.

Fig. 8 plots the throughput versus R for the proposed system with the TEP and EEP schemes, where $N = 30$ and $\frac{P_{AP}}{N_0} = 40$ dB. It can be observed that there exists an optimal value for R that maximizes the throughput. The reason behind this is that at low rates, the outage probability is low and the throughput is limited by R . In contrast, at high rates, the throughput is limited by the high outage probability. Hence, an optimal value of R that maximizes the throughput must exist. Moreover, it can be seen that for U_r the throughput performance of the TEP scheme is better than that of the EEP scheme for small values of R , while for U_t the EEP scheme outperforms the TEP scheme for large values of R .

Fig. 9 shows the throughput versus α_{AP}/α_{IT} of the proposed system with the TEP and EEP schemes, where $N = 30$, $\frac{P_{AP}}{N_0} = 35$ dB, $R = 2$, $\beta_{r,TEP} = \beta_{r,EEP} = 0.6$, and $\beta_{t,TEP} = \beta_{t,EEP} = 0.4$. It can be seen that the throughput increases first and then decreases with α_{AP}/α_{IT} . The reason lies in that there is a tradeoff between the ET and IT phases. For longer IT phases, more data can be transferred while the users harvest less energy and the transmission power is reduced. Moreover, it can be observed that the optimal duration for the IT phase is smaller for the far-side user U_r , compared to the near-side user U_t , since U_r needs more time in the ET phase to harvest energy. Furthermore, since the EEP scheme allocates more power to U_r , for U_r the EEP scheme performs

better than the TEP scheme while for U_t the TEP scheme outperforms the EEP scheme.

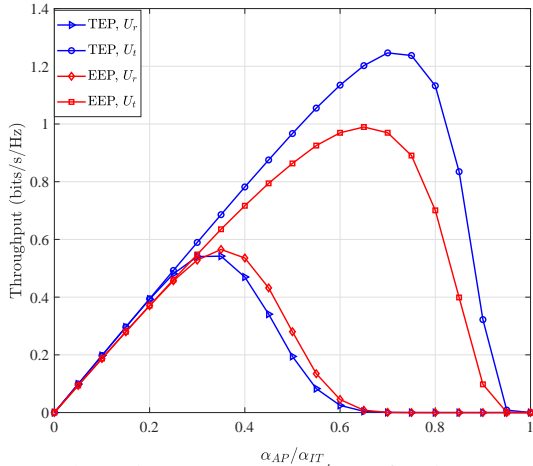


Fig. 9: Throughput versus α_{AP}/α_{IT} for the proposed system with the TEP and EEP schemes, where $N = 30$, $\frac{P_{AP}}{N_0} = 35$ dB, and $R = 2$.

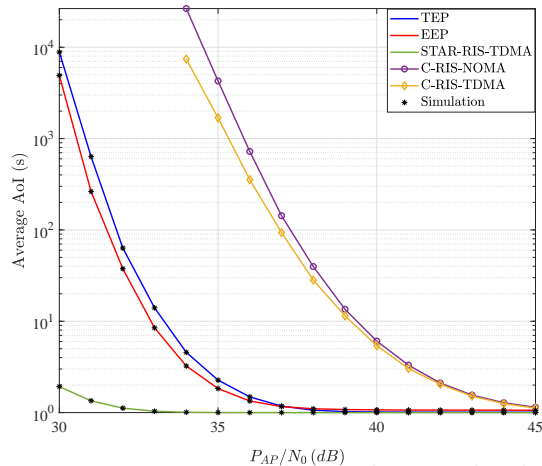


Fig. 10: Average AoI versus transmit SNR of various systems, where $N = 32$ and $R = 2$.

Fig. 10 plots the average AoI versus transmit SNR of various systems, where $N = 32$, $R = 2$, $\beta_{r,TEP} = \beta_{r,EEP} = 0.6$, and $\beta_{t,TEP} = \beta_{t,EEP} = 0.4$. It is observed that the performance of the STAR-RIS-TDMA scheme is better than that of the proposed system, since the STAR-RIS-TDMA scheme has no inter-user interference and better success probability. Moreover, it can be seen that there is an intersection between the TEP and EEP schemes. The average AoI of the EEP scheme is smaller than that of the TEP scheme at low SNRs, while the TEP scheme shows a better average AoI performance at high SNRs. This is because for low SNRs, the EEP scheme can allocate more power to U_r to reduce the performance gap between the two users, thus increasing the success probability. For high SNRs, the EEP scheme allocates excessive power to U_r , which deteriorates the performance in terms of average AoI.

Fig. 11 illustrates the average AoI versus energy-splitting ratio $\beta_{r,TEP}/\beta_{r,EEP}$ for the proposed system with the TEP and EEP schemes, where $N = 30$ and $R = 2$. It can be observed that for the EEP scheme, the optimal value of $\beta_{r,EEP}$ is about 0.6. The reason behind this is that low values of $\beta_{r,EEP}$ cause deteriorations in the average AoI due to poor performance for U_r , and high values of $\beta_{r,EEP}$ allocate excessive power to U_r , thus resulting in serious inter-user interference, which is not conducive to SIC decoding. Moreover, it can be seen that the TEP scheme yields better

performance most of the time. This is because the TEP scheme uses the time-switching protocol in the downlink, which balances the resource allocation and improves the performance of U_r for low values of $\beta_{r,TEP}$, and avoids excessive power allocation for high values of $\beta_{r,TEP}$.

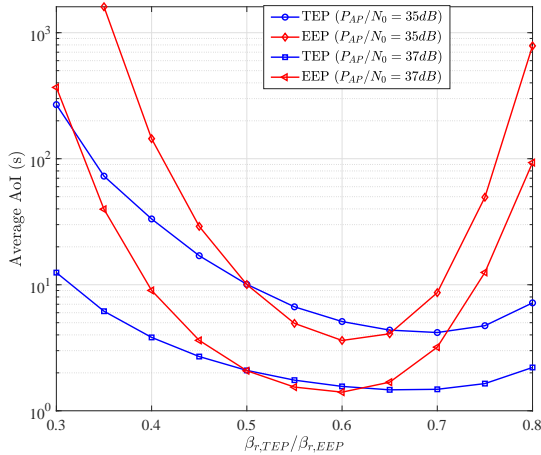


Fig. 11: Average AoI versus $\beta_{r,TEP}/\beta_{r,EEP}$ for the proposed system with the TEP and EEP schemes, where $N = 30$ and $R = 2$.

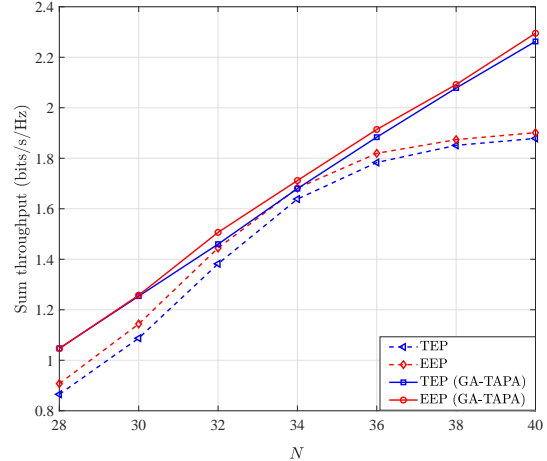


Fig. 12: Optimized sum throughput versus the number of STAR-RIS N for the proposed system with the EEP and TEP schemes, where $\frac{P_{AP}}{N_0} = 35$ dB and $R = 2$.

Fig. 12 shows the optimized sum throughput versus the number of the STAR-RIS N for the proposed system with EEP and TEP schemes, where $\frac{P_{AP}}{N_0} = 35$ dB and $R = 2$. It can be observed that our proposed GA-TAPA method outperforms the baseline TEP and EEP schemes. The GA-TAPA method can adjust the parameters to improve the sum throughput performance according to variations in N . For example, the TEP scheme with GA-TAPA method can achieve 1 dB gain at sum throughput of 1.2 compared to the TEP scheme. Moreover, it can be seen that when N becomes large, the growth in the sum throughput of the TEP and EEP schemes becomes smaller and tends to saturation while the TEP and EEP schemes with GA-TAPA method can adjust parameters and continue to improve the performance in terms of sum throughput.

VII. CONCLUSION

In this paper, a STAR-RIS aided wireless-powered NOMA system was proposed, where the TEP and EEP schemes are considered. The outage probability, sum throughput, and average AoI of the proposed system with the TEP and EEP schemes and the STAR-RIS aided wireless-powered

TDMA system were derived over Nakagami- m fading channels. Simulation and numerical results show that the proposed system with the TEP and EEP schemes not only yields better performance than baseline schemes, but also offers higher sum throughputs at the cost of the outage probability and average AoI compared to the STAR-RIS aided wireless-powered TDMA system. Moreover, the GA-TAPA algorithm has been designed to optimize the sum throughput while satisfying an average AoI constraint by jointly optimizing the time-allocation and power-allocation parameters. Results show that the proposed GA-TAPA method can significantly improve the sum throughput. Thanks to these advantages, the proposed STAR-RIS aided wireless-powered NOMA system can provide a new way to solve the multi-user interference and energy supply problems in the future IoT systems.

APPENDIX A

Here, the n -th moment of $H_{h_i g_{t,i}}$ is derived. Since $h_i \sim \text{Nakagami}(m_i, \Omega_i)$ and $g_{t,i} \sim \text{Nakagami}(m_{t,i}, \Omega_{t,i})$, the PDF of h_i and $g_{t,i}$ are given by

$$f_{h_i}(x; m_i, \Omega_i) = \frac{2m_i^{m_i}}{\Gamma(m_i)\Omega_i^{m_i}} x^{2m_i-1} e^{-\frac{m_i}{\Omega_i}x^2}, f_{g_{t,i}}(x; m_{t,i}, \Omega_{t,i}) = \frac{2m_{t,i}^{m_{t,i}}}{\Gamma(m_{t,i})\Omega_{t,i}^{m_{t,i}}} x^{2m_{t,i}-1} e^{-\frac{m_{t,i}}{\Omega_{t,i}}x^2}. \quad (41)$$

Considering $Z = XY$, $f_Z(z) = \int_0^\infty \frac{1}{x} f_Y\left(\frac{z}{x}\right) f_X(x) dx$. For $H_{h_i g_{t,i}} = h_i g_{t,i}$, the PDF of $H_{h_i g_{t,i}}$ is expressed as

$$f_{H_{h_i g_{t,i}}}(z) = \frac{4m_i^{m_i} m_{t,i}^{m_{t,i}}}{\Gamma(m_i)\Omega_i^{m_i} \Gamma(m_{t,i})\Omega_{t,i}^{m_{t,i}}} z^{2m_{t,i}-1} \int_0^\infty x^{2m_i-2m_{t,i}-1} e^{-\left(\frac{m_i}{\Omega_i}x^2 - \frac{m_{t,i}}{\Omega_{t,i}}\left(\frac{z}{x}\right)^2\right)} dx. \quad (42)$$

According to ([37], eq.(3.478.4)), (42) is reformulated as

$$f_{H_{h_i g_{t,i}}}(z) = \frac{4\lambda_{h_i g_{t,i}}^{m_i+m_{t,i}}}{\Gamma(m_i)\Gamma(m_{t,i})} z^{m_i+m_{t,i}-1} K_{m_i-m_{t,i}}(2z\lambda_{h_i g_{t,i}}), \quad (43)$$

where $\lambda_{h_i g_{t,i}} = \sqrt{\frac{m_i}{\Omega_i} \frac{m_{t,i}}{\Omega_{t,i}}}$.

The n -th moment of $H_{h_i g_{t,i}}$ is defined as $\mu_{H_{h_i g_{t,i}}}(n) \triangleq E\left(H_{h_i g_{t,i}}^n\right) = \int_0^\infty z^n f_{H_{h_i g_{t,i}}}(z) dz$. Using (43) and after some mathematical manipulations, $\mu_{H_{h_i g_{t,i}}}(n)$ is obtained as

$$\mu_{H_{h_i g_{t,i}}}(n) = \lambda_{h_i g_{t,i}}^{-n} \frac{\Gamma(m_i + n/2) \Gamma(m_{t,i} + n/2)}{\Gamma(m_i) \Gamma(m_{t,i})}. \quad (44)$$

APPENDIX B

Here, (23) is derived. Let $A = \frac{P_{AP} l_t^2 \beta_{t,TEP} \alpha_t}{\alpha_{AP} N_0}$, $B = \frac{P_{AP} l_r^2 \beta_{r,TEP} \alpha_r}{\alpha_{AP} N_0}$, the first part of (23), termed as P_1 , can be written as

$$\begin{aligned}
P_1 &= \Pr \left(\frac{\gamma_{t,TEP}}{\gamma_{r,TEP} + 1} < \gamma_{th}, \frac{\gamma_{r,TEP}}{\gamma_{t,TEP} + 1} < \gamma_{th} \right) = \Pr \left(\frac{A |G_{h_i g_{t,i}}|^4}{B |G_{h_i g_{r,i}}|^4 + 1} < \gamma_{th}, \frac{B |G_{h_i g_{r,i}}|^4}{A |G_{h_i g_{t,i}}|^4 + 1} < \gamma_{th} \right) \\
&= \Pr \left(\frac{B |G_{h_i g_{r,i}}|^4}{A \gamma_{th}} - \frac{1}{A} < |G_{h_i g_{t,i}}|^4 < \frac{\gamma_{th}}{A} (B |G_{h_i g_{r,i}}|^4 + 1) \right) \\
&= F \left(\frac{\gamma_{th}}{A} (B |G_{h_i g_{r,i}}|^4 + 1) \right) - F \left(\frac{B |G_{h_i g_{r,i}}|^4}{A \gamma_{th}} - \frac{1}{A} \right) \\
&= \int_0^{\infty} F \left(\frac{\gamma_{th}}{A} (Bx + 1) \right) f(x) dx - \int_{\frac{\gamma_{th}}{B}}^{\infty} F \left(\frac{Bx}{A \gamma_{th}} - \frac{1}{A} \right) f(x) dx. \tag{45}
\end{aligned}$$

The first integral in (45) can be calculated as

$$\begin{aligned}
\int_0^{\infty} F \left(\frac{\gamma_{th}}{A} (Bx + 1) \right) f(x) dx &= \int_0^{\infty} \frac{1}{\Gamma(Nk)} \gamma \left(Nk, \theta \left(\frac{\gamma_{th}}{A} (Bx + 1) \right)^{\frac{1}{4}} \right) \frac{\theta^{Nk} e^{-\theta x^{\frac{1}{4}}} x^{\frac{Nk-4}{4}}}{4(Nk-1)!} dx \\
&= 1 - \sum_{m=0}^{Nk-1} \frac{\theta^{Nk+m}}{4m! (Nk-1)!} \int_0^{\infty} e^{-\theta \left(\frac{\gamma_{th}}{A} (Bx+1) \right)^{\frac{1}{4}}} \left(\frac{\gamma_{th}}{A} (Bx+1) \right)^{\frac{m}{4}} e^{-\theta x^{\frac{1}{4}}} x^{\frac{Nk-4}{4}} dx. \tag{46}
\end{aligned}$$

Furthermore, (46) is evaluated by leveraging the Gauss-Hermite quadrature approach. According to Table (25.10) in [43], one has

$$\int_{-\infty}^{\infty} g(x) dx = \sum_{w=1}^W \psi_w g(x_w) \exp(x_w^2) + O_W, \tag{47}$$

where W denotes the number of sample points used for approximation, x_w is the w -th root of the Hermite polynomial $H_W(x)$ ($w = 1, 2, \dots, W$), ψ_w is the w -th associated weight obtained from $\frac{2^{W-1} W! \sqrt{\pi}}{W^2 H_{W-1}^2(x_w)}$ and O_W is the residual term that tends to 0 when W tends to infinity.

Using variable substitution $\ln(x) = u$ to obtain the new limits with integral from $-\infty$ to $+\infty$ and after some mathematical operations, one obtains

$$\begin{aligned}
&\int_0^{\infty} F \left(\frac{\gamma_{th}}{A} (Bx + 1) \right) f(x) dx \\
&\approx 1 - \sum_{m=0}^{Nk-1} \frac{\theta^{Nk+m}}{4m! (Nk-1)!} \sum_{w=1}^W \psi_w e^{-\theta \left(\frac{\gamma_{th}}{A} (B e^{u_w} + 1) \right)^{\frac{1}{4}}} \left(\frac{\gamma_{th}}{A} (B e^{u_w} + 1) \right)^{\frac{m}{4}} e^{-\theta e^{\frac{u_w}{4}}} e^{u_w \frac{Nk-4}{4}} e^{u_w + u_w^2} - O_W. \tag{48}
\end{aligned}$$

The second integral in (45) can be calculated as

$$\begin{aligned} \int_{\frac{\gamma th}{B}}^{\infty} F\left(\frac{Bx}{A\gamma th} - \frac{1}{A}\right) f(x) dx &= \int_{\frac{\gamma th}{B}}^{\infty} \frac{1}{\Gamma(Nk)} \gamma\left(Nk, \theta\left(\frac{Bx}{A\gamma th} - \frac{1}{A}\right)^{\frac{1}{4}}\right) \frac{\theta^{Nk} e^{-\theta x^{\frac{1}{4}}} x^{\frac{Nk-4}{4}}}{4(Nk-1)!} dx \\ &= 1 - F\left(\frac{\gamma th}{B}\right) - \sum_{m=0}^{Nk-1} \frac{\theta^{Nk+m}}{4m!(Nk-1)!} \int_{\frac{\gamma th}{B}}^{\infty} e^{-\theta\left(\frac{Bx}{A\gamma th} - \frac{1}{A}\right)^{\frac{1}{4}}} \left(\frac{Bx}{A\gamma th} - \frac{1}{A}\right)^{\frac{m}{4}} e^{-\theta x^{\frac{1}{4}}} x^{\frac{Nk-4}{4}} dx. \end{aligned} \quad (49)$$

Similarly, using variable substitution $\ln\left(x - \frac{\gamma th}{B}\right) = u$ to obtain the new limits with integral from $-\infty$ to $+\infty$ and after some mathematical operations, one obtains

$$\begin{aligned} \int_{\frac{\gamma th}{B}}^{\infty} F\left(\frac{Bx}{A\gamma th} - \frac{1}{A}\right) f(x) dx &\approx 1 - F\left(\frac{\gamma th}{B}\right) - \sum_{m=0}^{Nk-1} \frac{\theta^{Nk+m}}{4m!(Nk-1)!} \sum_{w=1}^W \psi_w e^{-\theta\left(\frac{B(e^{u_w} + \frac{\gamma th}{B})}{A\gamma th} - \frac{1}{A}\right)^{\frac{1}{4}}} \\ &\times \left(\frac{B(e^{u_w} + \frac{\gamma th}{B})}{A\gamma th} - \frac{1}{A}\right)^{\frac{m}{4}} e^{-\theta(e^{u_w} + \frac{\gamma th}{B})^{\frac{1}{4}}} \left(e^{u_w} + \frac{\gamma th}{B}\right)^{\frac{Nk-4}{4}} e^{u_w + u_w^2} - O_W. \end{aligned} \quad (50)$$

Then, the second part of (23), termed as P_2 , can be computed as

$$\begin{aligned} P_2 &= \Pr\left(A|G_{h_i g_t, i}|^4 < \gamma th, \frac{B|G_{h_i g_r, i}|^4}{A|G_{h_i g_t, i}|^4 + 1} \geq \gamma th\right) = \Pr\left(|G_{h_i g_t, i}|^4 < \frac{\gamma th}{A}, |G_{h_i g_r, i}|^4 \geq \frac{\gamma th}{B} (A|G_{h_i g_t, i}|^4 + 1)\right) \\ &= \int_0^{\frac{\gamma th}{A}} 1 - F\left(\frac{\gamma th}{B} (Ax + 1)\right) f(x) dx = \sum_{m=0}^{Nk-1} \frac{\theta^{Nk+m}}{4m!(Nk-1)!} \int_0^{\frac{\gamma th}{A}} e^{-\theta\left(\frac{\gamma th}{B} (Ax+1)\right)^{\frac{1}{4}}} \left(\frac{\gamma th}{B} (Ax + 1)\right)^{\frac{m}{4}} e^{-\theta x^{\frac{1}{4}}} x^{\frac{Nk-4}{4}} dx. \end{aligned} \quad (51)$$

Using (48), (50), and (51), (23) can be derived.

APPENDIX C

First, we derive the success probability Φ_{TEP} of the TEP scheme. Since the data of both U_r and U_t have to be successfully decoded, Φ_{TEP} is expressed as

$$\Phi_{TEP} = \Pr\left(\frac{\gamma_{r,TEP}}{\gamma_{t,TEP} + 1} > \gamma_{th}, \gamma_{t,TEP} > \gamma_{th}, \gamma_{r,EEP} \geq \gamma_{t,EEP}\right) + \Pr\left(\frac{\gamma_{t,TEP}}{\gamma_{r,TEP} + 1} > \gamma_{th}, \gamma_{r,TEP} > \gamma_{th}, \gamma_{t,EEP} \geq \gamma_{r,EEP}\right). \quad (52)$$

Let $U_1 = P_{AP} l_r^2 \beta_{r,TEP} \alpha_r$, $U_2 = P_{AP} l_t^2 \beta_{t,TEP} \alpha_t$, the first part of (52), termed as Φ_1 , is calculated

as

$$\begin{aligned} \Phi_1 &= \Pr\left(|G_{h_i g_r, i}|^4 > \frac{\gamma_{th}(U_2 |G_{h_i g_t, i}|^4 + \alpha_{AP} N_0)}{U_1}, |G_{h_i g_t, i}|^4 > \frac{\gamma_{th} \alpha_{AP} N_0}{U_2}, |G_{h_i g_r, i}|^4 > \frac{U_2 |G_{h_i g_t, i}|^4}{U_1}\right) \\ &= \Pr\left(|G_{h_i g_r, i}|^4 > \frac{\gamma_{th}(U_2 |G_{h_i g_t, i}|^4 + \alpha_{AP} N_0)}{U_1}, |G_{h_i g_t, i}|^4 > \frac{\gamma_{th} \alpha_{AP} N_0}{U_2}\right) \end{aligned}$$

$$\begin{aligned}
&= \int_{\frac{\gamma_{th}\alpha_{AP}N_0}{U_2}}^{\infty} \left(1 - F\left(\frac{\gamma_{th}(U_2x + \alpha_{AP}N_0)}{U_1}\right)\right) f(x) dx \\
&= \int_{\frac{\gamma_{th}\alpha_{AP}N_0}{U_2}}^{\infty} \left[e^{-\left(\frac{\theta^4\gamma_{th}(U_2x + \alpha_{AP}N_0)}{U_1}\right)^{\frac{1}{4}}} \sum_{m=0}^{Nk-1} \frac{\left(\frac{\theta^4\gamma_{th}(U_2x + \alpha_{AP}N_0)}{U_1}\right)^{\frac{m}{4}}}{m!} \right] \frac{\theta^{Nk} e^{-\theta x^{\frac{1}{4}}} x^{\frac{Nk-4}{4}}}{4(Nk-1)!} dx \\
&= \sum_{m=0}^{Nk-1} \frac{\theta^{Nk}}{4(Nk-1)!m!} \int_{\frac{\gamma_{th}\alpha_{AP}N_0}{U_2}}^{\infty} e^{-\left(\frac{\theta^4\gamma_{th}(U_2x + \alpha_{AP}N_0)}{U_1}\right)^{\frac{1}{4}}} \left(\frac{\theta^4\gamma_{th}(U_2x + \alpha_{AP}N_0)}{U_1}\right)^{\frac{m}{4}} e^{-\theta x^{\frac{1}{4}}} x^{\frac{Nk-4}{4}} dx. \tag{53}
\end{aligned}$$

Similar to (50), using variable substitution $\ln\left(x - \frac{\gamma_{th}\alpha_{AP}N_0}{U_2}\right) = u$ to obtain the new limits with integral from $-\infty$ to $+\infty$ and after some mathematical operations, one obtains

$$\begin{aligned}
\Phi_1 &= \sum_{m=0}^{Nk-1} \frac{\theta^{Nk}}{4(Nk-1)!m!} \sum_{w=1}^W \psi_w e^{-\left(\frac{\theta^4\gamma_{th}U_3}{U_1}\right)^{\frac{1}{4}}} \left(\frac{\theta^4\gamma_{th}U_3}{U_1}\right)^{\frac{m}{4}} e^{-\theta\left(e^{u_w} + \frac{\gamma_{th}\alpha_{AP}N_0}{U_2}\right)^{\frac{1}{4}}} \\
&\quad \times \left(e^{u_w} + \frac{\gamma_{th}\alpha_{AP}N_0}{U_2}\right)^{\frac{Nk-4}{4}} e^{u_w + u_w^2} + O_W, \tag{54}
\end{aligned}$$

where $U_3 = U_2e^{u_w} + \gamma_{th}\alpha_{AP}N_0 + \alpha_{AP}N_0$.

Using the same method, the second part of (52), termed as Φ_2 , is calculated as

$$\begin{aligned}
\Phi_2 &= \sum_{m=0}^{Nk-1} \frac{\theta^{Nk}}{4(Nk-1)!m!} \sum_{w=1}^W \psi_w e^{-\left(\frac{\theta^4\gamma_{th}U_4}{U_2}\right)^{\frac{1}{4}}} \left(\frac{\theta^4\gamma_{th}U_4}{U_2}\right)^{\frac{m}{4}} e^{-\theta\left(e^{u_w} + \frac{\gamma_{th}\alpha_{AP}N_0}{U_1}\right)^{\frac{1}{4}}} \\
&\quad \times \left(e^{u_w} + \frac{\gamma_{th}\alpha_{AP}N_0}{U_1}\right)^{\frac{Nk-4}{4}} e^{u_w + u_w^2} + O_W, \tag{55}
\end{aligned}$$

where $U_4 = U_1e^{u_w} + \gamma_{th}\alpha_{AP}N_0 + \alpha_{AP}N_0$. Using (54) and (55), (36) can be obtained.

The success probability Φ_T of the STAR-RIS aided wireless-powered TDMA system is expressed as

$$\Phi_T = \Pr(\gamma_r > \gamma_t, \gamma_t > \gamma_{th}) + \Pr(\gamma_t > \gamma_r, \gamma_r > \gamma_{th}). \tag{56}$$

The first term of (56), termed as $\Phi_{T,1}$, is calculated as

$$\begin{aligned}
\Phi_{T,1} &= \Pr\left(\frac{P_{AP}l_r^2|G_{h_i g_r, i}|^4\alpha_r}{\alpha_{AP}^r N_0} > \frac{P_{AP}l_t^2|G_{h_i g_t, i}|^4\alpha_t}{\alpha_{AP}^t N_0}, \frac{P_{AP}l_t^2|G_{h_i g_t, i}|^4\alpha_t}{\alpha_{AP}^t N_0} > \gamma_{th}\right) \\
&= \Pr\left(\frac{\gamma_{th}\alpha_{AP}^t N_0}{P_{AP}l_t^2\alpha_t} < |G_{h_i g_t, i}|^4 < \frac{l_r^2|G_{h_i g_r, i}|^4\alpha_r\alpha_{AP}^t}{\alpha_{AP}^r l_t^2\alpha_t}\right) = F(U_5|G_{h_i g_r, i}|^4) - F\left(\frac{\gamma_{th}\alpha_{AP}^t N_0}{P_{AP}l_t^2\alpha_t}\right), \tag{57}
\end{aligned}$$

where $U_5 = \frac{l_r^2\alpha_r\alpha_{AP}^t}{\alpha_{AP}^r l_t^2\alpha_t}$.

$F(U_5|G_{h_i g_r, i}|^4)$ as the first term of (57), termed as $\Phi_{T,1}^1$, can be further expressed as

$$\Phi_{T,1}^1 = \int_0^\infty F(U_5 x) f(x) dx = 1 - \sum_{m=0}^{Nk-1} \frac{\theta^{m+Nk}}{m! 4^{(Nk-1)!}} \int_0^\infty e^{-\theta(U_5 x)^{\frac{1}{4}}} (U_5 x)^{\frac{m}{4}} e^{-\theta x^{\frac{1}{4}}} x^{\frac{Nk-4}{4}} dx. \quad (58)$$

Let $x^{\frac{1}{4}} = t$, (58) can be written as

$$\Phi_{T,1}^1 = 1 - \sum_{m=0}^{Nk-1} \frac{\theta^{m+Nk} U_5^{\frac{m}{4}}}{m! (Nk-1)!} \int_0^\infty e^{-\theta(U_5^{\frac{1}{4}}+1)t} t^{Nk+m-1} dt. \quad (59)$$

Using (3.478) in [37], one has

$$\Phi_{T,1}^1 = 1 - \sum_{m=0}^{Nk-1} \frac{\theta^{m+Nk} U_5^{\frac{m}{4}}}{m! (Nk-1)!} \left(\theta \left(U_5^{\frac{1}{4}} + 1 \right) \right)^{-(Nk+m)} \Gamma(Nk+m). \quad (60)$$

The second part of (56), termed as $\Phi_{T,2}$, can be calculated in a similar manner, given by

$$\Phi_{T,2} = 1 - \sum_{m=0}^{Nk-1} \frac{\theta^{m+Nk} U_6^{\frac{m}{4}}}{m! (Nk-1)!} \left(\theta \left(U_6^{\frac{1}{4}} + 1 \right) \right)^{-(Nk+m)} \Gamma(Nk+m) - F \left(\frac{\gamma_{th} \alpha_r}{P_{AP} l_r^2 \alpha_r} \right), \quad (61)$$

where $U_6 = \frac{l_t^2 \alpha_t \alpha_r}{\alpha_{AP}^2 l_r^2 \alpha_r}$. Using (57), (60), and (61), (38) can be obtained.

REFERENCES

- [1] B. Clerckx, K. Huang, L. Varshney, S. Ulukus, and M. Alouini, "Wireless power transfer for future networks: Signal processing, machine learning, computing, and sensing," *IEEE J. Sel. Topics Signal Process.*, vol. 15, no. 5, pp. 1060–1094, Aug. 2021.
- [2] P. Wu, F. Xiao, H. Huang, C. Sha, and S. Yu, "Adaptive and extensible energy supply mechanism for uavs-aided wireless-powered internet of things," *IEEE Internet Things J.*, vol. 7, no. 9, pp. 9201–9213, Sept. 2020.
- [3] K. Moon, K. Kim, Y. Kim, and T. Lee, "Device-selective energy request in RF energy-harvesting networks," *IEEE Commun. Lett.*, vol. 25, no. 5, pp. 1716–1719, May. 2021.
- [4] Y. Wang, K. Yang, W. Wan, Y. Zhang, and Q. Liu, "Energy-efficient data and energy integrated management strategy for IoT devices based on RF energy harvesting," *IEEE Internet Things J.*, vol. 8, no. 17, pp. 13640–13651, Sept. 2021.
- [5] H. Ko, S. Pack, and V. Leung, "Energy utilization-aware operation control algorithm in energy harvesting base stations," *IEEE Internet Things J.*, vol. 6, no. 6, pp. 10824–10833, Dec. 2019.
- [6] Y. Zheng, J. Hu, and K. Yang, "Average age of information in wireless powered relay aided communication network," *IEEE Internet Things J.*, vol. 9, no. 13, pp. 11311–11323, Jul. 2022.
- [7] L. Xie, J. Xu, and Y. Zeng, "Common throughput maximization for uav-enabled interference channel with wireless powered communications," *IEEE Trans. Commun.*, vol. 68, no. 5, pp. 3197–3212, May. 2020.
- [8] Y. Zheng, S. Bi, Y. Zhang, X. Lin, and H. Wang, "Joint beamforming and power control for throughput maximization in IRS-assisted MISO WPCNs," *IEEE Internet Things J.*, vol. 8, no. 10, pp. 8399–8410, May. 2021.
- [9] O. Waqar and R. Adve, "On the throughput of wireless powered communication systems with a multiple antenna bidirectional relay," *IEEE Commun. Lett.*, vol. 8, no. 3, pp. 941–944, Jun. 2019.
- [10] S. Van, H. Ngo, and S. Cotton, "Wireless powered wearables using distributed massive MIMO," *IEEE Trans. Commun.*, vol. 68, no. 4, pp. 2156–2172, Apr. 2020.
- [11] J. He, H. Wymeersch, and M. Juntti, "Channel estimation for RIS-aided mmWave MIMO systems via atomic norm minimization," *IEEE Trans. Wireless Commun.*, vol. 20, no. 9, pp. 5786–5797, Sept. 2021.
- [12] T. Do, G. Kaddoum, T. Nguyen, D. da Costa, and Z. Haas, "Multi-RIS-aided wireless systems: Statistical characterization and performance analysis," *IEEE Trans. Commun.*, vol. 69, no. 12, pp. 8641–8658, Dec. 2021.
- [13] Q. Wu, S. Zhang, B. Zheng, C. You, and R. Zhang, "Intelligent reflecting surface-aided wireless communications: A tutorial," *IEEE Trans. Commun.*, vol. 69, no. 5, pp. 3313–3351, May. 2021.
- [14] Y. Zheng, S. Bi, Y. Zhang, Z. Quan, and H. Wang, "Intelligent reflecting surface enhanced user cooperation in wireless powered communication networks," *IEEE Wireless Commun. Lett.*, vol. 9, no. 6, pp. 901–905, Jun. 2020.
- [15] Z. Chu, Z. Zhu, F. Zhou, M. Zhang, and N. Al-Dhahir, "Intelligent reflecting surface assisted wireless powered sensor networks for internet of things," *IEEE Trans. Commun.*, vol. 69, no. 7, pp. 4877–4889, Jul. 2021.
- [16] K. Xie, G. Cai, and G. Kaddoum, "Design and performance analysis of RIS-aided DCSK-WPC system with energy buffer," *IEEE Trans. Commun.*, early access, Jan. 2023, doi: 10.1109/TCOMM.2023.3234995.

- [17] S. Gong, C. Xing, S. Wang, L. Zhao, and J. An, "Throughput maximization for intelligent reflecting surface aided MIMO WPCNs with different DL/UL reflection patterns," *IEEE Trans. Signal Process.*, vol. 69, pp. 2706–2724, Apr. 2021.
- [18] Y. Han, N. Li, Y. Liu, T. Zhang, and X. Tao, "Artificial noise aided secure NOMA communications in STAR-RIS networks," *IEEE Wireless Commun. Lett.*, vol. 11, no. 6, pp. 1191–1195, Jun. 2022.
- [19] J. Xu, Y. Liu, X. Mu, and O. Dobre, "STAR-RISs: Simultaneous transmitting and reflecting reconfigurable intelligent surfaces," *IEEE Commun. Lett.*, vol. 25, no. 9, pp. 3134–3138, Sept. 2021.
- [20] Y. Liu, X. Mu, J. Xu, R. Schober, Y. Hao, H. Poor, and L. Hanzo, "STAR: Simultaneous transmission and reflection for 360° coverage by intelligent surfaces," *IEEE Wireless Commun.*, vol. 28, no. 6, pp. 102–109, Dec. 2021.
- [21] C. Wu, X. Mu, Y. Liu, X. Gu, and X. Wang, "Resource allocation in STAR-RIS-aided networks: OMA and NOMA," *IEEE Trans. Wireless Commun.*, vol. 21, no. 9, pp. 7653–7667, Sept. 2022.
- [22] X. Mu, Y. Liu, L. Guo, J. Lin, and R. Schober, "Simultaneously transmitting and reflecting (STAR) RIS aided wireless communications," *IEEE Trans. Wireless Commun.*, vol. 21, no. 5, pp. 3083–3098, May. 2022.
- [23] C. Wu, Y. Liu, X. Mu, X. Gu, and O. Dobre, "Coverage characterization of STAR-RIS networks: NOMA and OMA," *IEEE Commun. Lett.*, vol. 25, no. 9, pp. 3036–3040, Sept. 2021.
- [24] X. Qin, Z. Song, T. Hou, W. Yu, J. Wang, and X. Sun, "Joint resource allocation and configuration design for STAR-RIS-enhanced wireless-powered MEC," *arXiv:2208.13970*, 2022.
- [25] Z. Xie, W. Yi, X. Wu, Y. Liu, and A. Nallanathan, "STAR-RIS aided NOMA in multicell networks: A general analytical framework with gamma distributed channel modeling," *IEEE Trans. Commun.*, vol. 70, no. 8, pp. 5629–5644, Aug. 2022.
- [26] Z. Ding, Z. Yang, P. Fan, and H. Poor, "On the performance of non-orthogonal multiple access in 5G systems with randomly deployed users," *IEEE Signal Process. Lett.*, vol. 21, no. 12, pp. 1501–1505, Dec. 2014.
- [27] S. Islam, N. Avazov, O. Dobre, and K. Kwak, "Power-domain non-orthogonal multiple access (NOMA) in 5G systems: Potentials and challenges," *IEEE Commun. Surveys Tuts.*, vol. 19, no. 2, pp. 721–742, 2017.
- [28] C. Zhang, W. Yi, Y. Liu, Z. Ding, and L. Song, "STAR-IOs aided NOMA networks: Channel model approximation and performance analysis," *IEEE Trans. Wireless Commun.*, vol. 21, no. 9, pp. 6861–6876, Sept. 2022.
- [29] T. Wang, M. Badiu, G. Chen, and J. Coon, "Outage probability analysis of STAR-RIS assisted NOMA network with correlated channels," *IEEE Commun. Lett.*, vol. 26, no. 8, pp. 1774–1778, Aug. 2022.
- [30] M. Aldababsa, A. Khaleel, and E. Basar, "STAR-RIS-NOMA networks: An error performance perspective," *IEEE Commun. Lett.*, vol. 26, no. 8, pp. 1784–1788, Aug. 2022.
- [31] Q. Gu, G. Wang, R. Fan, F. Li, H. Jiang, and Z. Zhong, "Optimal resource allocation for wireless powered sensors: A perspective from age of information," *IEEE Commun. Lett.*, vol. 24, no. 11, pp. 2559–2563, Nov. 2020.
- [32] S. Kaul, R. Yates, and M. Gruteser, "Real-time status: How often should one update?" in *Proc. IEEE INFOCOM*, Orlando, FL, USA, pp. 2731–2735, Mar. 2012.
- [33] C. Wu, C. You, Y. Liu, X. Gu, and Y. Cai, "Channel estimation for STAR-RIS-aided wireless communication," *IEEE Commun. Lett.*, vol. 26, no. 3, pp. 652–656, Mar. 2022.
- [34] S. Tegos, P. Diamantoulakis, A. Lioumpas, P. Sarigiannidis, and G. Karagiannidis, "Slotted ALOHA with NOMA for the next generation IoT," *IEEE Trans. Commun.*, vol. 68, no. 10, pp. 6289–6301, Oct. 2020.
- [35] S. Atapattu, R. Fan, P. Dharmawansa, G. Wang, J. Evans, and T. Tsiftsis, "Reconfigurable intelligent surface assisted two-way communications: Performance analysis and optimization," *IEEE Trans. Commun.*, vol. 68, no. 10, pp. 6552–6567, Oct. 2020.
- [36] I. Krikidis, "Average age of information in wireless powered sensor networks," *IEEE Wireless Commun. Lett.*, vol. 8, no. 2, pp. 628–631, Apr. 2019.
- [37] I. S. Gradshteyn and I. M. Ryzhik, *Table of integrals, series, and products*, 2004.
- [38] A. Kosta, N. Pappas, and V. Angelakis, "Age of information: A new concept, metric, and tool," *Found. Trends Netw.*, vol. 12, no. 3, pp. 162–259, 2017.
- [39] L. He, M. Wen, Y. Chen, M. Yan, and B. Jiao, "Delay aware secure offloading for NOMA-assisted mobile edge computing in internet of vehicles," *IEEE Trans. Commun.*, vol. 70, no. 8, pp. 5271–5284, Aug. 2022.
- [40] F. Guo, H. Zhang, H. Ji, X. Li, and V. Leung, "An efficient computation offloading management scheme in the densely deployed small cell networks with mobile edge computing," *IEEE/ACM Trans. Netw.*, vol. 26, no. 6, pp. 2651–2664, Dec. 2018.
- [41] W. Xu, G. Cai, Y. Fang, S. Mumtaz, and G. Chen, "Performance analysis and resource allocation for a relaying LoRa system considering random nodal distances," *IEEE Trans. Commun.*, vol. 70, no. 3, pp. 1638–1652, Mar. 2022.
- [42] Z. Zhang, J. Chen, Y. Liu, Q. Wu, B. He, and L. Yang, "On the secrecy design of STAR-RIS assisted uplink NOMA networks," *IEEE Trans. Wireless Commun.*, vol. 21, no. 12, pp. 11207–11221, Dec. 2022.
- [43] M. Abramowitz, I. A. Stegun, and J. E. Romain, *Handbook of mathematical functions with formulas graphs and mathematical tables*. New York: NY, USA: Dover, 1965.